ADVANCED FUNCTIONAL MATERIALS
www.afm-journal.de

Recent Advancement in 2D Metal–Organic Framework for Environmental Remediation: A Review

Lun Lu, Liangzhong Li, Mengxu Chu, Cheng Chen, Boya Wang, Jun Wang, Yi Shen, Ruixue Ma, Bisheng Li, Liguo Shen, Hongjun Lin,* and Banglin Chen**

In a time characterized by the increasing interest in metal–organic frameworks (MOFs) as widely researched crystalline porous substances geared toward enhancing device and system capabilities across diverse environmental contexts, 2D MOFs emerge as a noteworthy class of nanomaterials that integrate the benefits of 2D structures with the unique characteristics inherent to MOFs. These 2D MOFs possess ultrathin nanosheet configuration, abundant accessible active sites, and remarkable mechanical flexibility. Such distinctive properties differentiate them from bulk MOFs and other 2D materials, offering the potential to instigate novel environmental phenomena and applications. This review focuses on the latest progress in the application of 2D MOFs within essential water-related ecological fields, including contaminant adsorption, photocatalytic degradation, membrane separation, environmental sensing, and disinfection. A variety of synthesis approaches for 2D MOFs are analyzed, accompanied by a discussion on their effectiveness across different environmental settings. The unique structure and features of 2D MOFs that grant outstanding environmental functionalities are compared with those of bulk MOFs. The environmental ramifications of 2D MOFs are highlighted while outlining future research needs to explore the environmental applications of these innovative materials.

1. Introduction

Over the past two decades, extensive research has focused on exploring nanomaterials to provide innovative solutions or improve existing ones for a wide range of urgent environmental issues, from water scarcity to air pollution.[1] Particularly, environmentally functional nanomaterials based on metal–organic frameworks (MOFs), including original bulk MOFs, MOF membranes, and MOF aerogels, have garnered considerable interest. These MOF-based materials possess distinctive features, including a large specific surface area, customizable inner and outer surface compositions, and adaptable structures.[2] Over time, MOFs-based nanomaterials have been widely used in various environmental applications, such as pollutant adsorption, photocatalytic degradation, sensing technologies, membrane separations, and sterilization procedures.[3]

L. Lu, M. Chu, R. Ma
State Environmental Protection Key Laboratory of Environmental Pollution Health Risk Assessment, South China Institute of Environmental Sciences
Ministry of Ecology and Environment
Guangzhou 510655, China

L. Lu, L. Li
Guangdong Provincial Key Laboratory of High-Quality Recycling of End-of-Life New Energy Devices, Guangzhou Institute of Energy Conversion
Chinese Academy of Sciences
Guangzhou 510640, China

M. Chu, J. Wang
State Key Laboratory of Separation Membranes and Membrane Processes, School of Environmental Science and Engineering
Tiangong University
Tianjin 300387, China

C. Chen, B. Wang, B. Li, L. Shen, H. Lin, B. Chen
Key Laboratory of Watershed Earth Surface Processes and Ecological Security, College of Geography and Environmental Sciences
Zhejiang Normal University
Jinhua 321004, China
E-mail: chencheng@zjnu.edu.cn; hjlin@zjnu.cn; Banglin.chen@fjnu.edu.cn

Y. Shen
Key Laboratory of Microbial Technology for Industrial Pollution Control of Zhejiang Province, College of Environment
Zhejiang University of Technology
Hangzhou 310032, China

B. Chen
Fujian Key Laboratory of Polymer Materials, College of Chemistry and Materials Science
Fujian Normal University
Fuzhou, Fujian, China

The ORCID identification number(s) for the author(s) of this article can be found under https://doi.org/10.1002/adfm.202419433

DOI: 10.1002/adfm.202419433

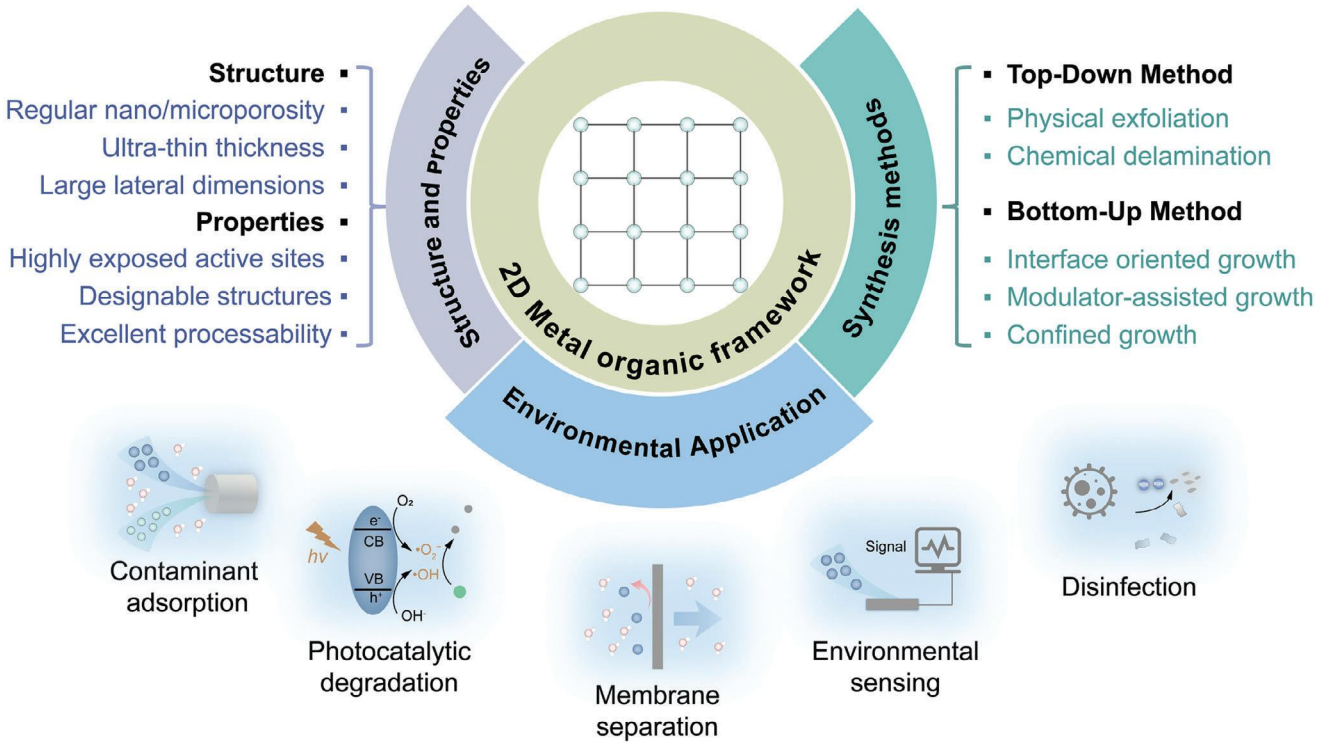

Figure 1. Schematic outline of this review.

The term "metal–organic framework" was first coined by Omar M. Yaghi in 1995 and has long been considered an ideal porous material for gas adsorption.[4] The broad spectrum of metal nodes and organic ligands, in conjunction with a variety of coordination geometries, has significantly advanced the development of an extensive array of bulk MOF crystals and nanocrystals (0D MOF nanoparticles and 1D MOF nanorods/nanowires) exhibiting diverse properties.[5] However, achieving precise control over the nanoscale growth of MOF crystals only in the lateral dimension without affecting the vertical dimension presented a challenge. It wasn't until 2008 that Qiu et al. introduced the first 2D MOF nanosheets.[6] Subsequently, a variety of 2D MOFs with diverse structures and characteristics quickly emerged. In the past decade, a range of 2D MOF nanosheets have been successfully produced mainly through top–down and bottom–up approaches.[7] These ultrathin 2D MOF nanosheets amalgamate the advantages of typical 2D materials with the distinctive attributes of MOFs. They not only exhibit the high surface-to-volume ratio and atomic thickness characteristic of 2D materials but also possess unique pore structures, tunable pore sizes, and abundant modification/functionalization surface sites. In comparison to bulk MOF crystals, 0D MOF nanoparticles, and 1D MOF nanorods/nanowires, their ultrathin nanosheet architecture, highly accessible active sites, and exceptional mechanical flexibility have garnered increasing attention across various application fields.[8] With demonstrated applications in electronics, catalysis, biomedicine, and energy-related fields, their potential in various environmental areas has become apparent.[9]

Although significant advancements have been made in the realm of 2D MOF nanosheets, existing literature extensively addresses their synthesis techniques, structural design, and applications in electrocatalysis and optics.[7c,10] However, there remains a notable deficiency in the comprehensive review pertaining to the preparation methods of 2D MOF nanosheets, as well as their applications and environmental impacts in pollution remediation. This comprehensive review seeks to consolidate the application of 2D MOF nanosheets in prospective environmental contexts. To begin with, the review delineates the structure, characteristics, and synthesis methods associated with 2D MOF nanosheets. Following this, a critical analysis of recent developments in various environmental applications of these nanosheets is presented, with an emphasis on water-related applications such as pollutant adsorption, photocatalysis, membrane separation, sensing, and disinfection (**Figure 1**). Particular focus is placed on the distinctive properties and environmental efficacy of 2D MOFs in comparison to bulk MOFs. In conclusion, the review underscores the implications of introducing 2D MOF nanosheets into the environment and outlines prospective research avenues necessary to enhance their environmental performance.

2. Structure and Properties of 2D MOFs

2.1. Structure

MOFs are crystalline compounds composed of organic linkers and infinite lattices or secondary building units (SBUs, metal ions, or clusters) interconnected via moderately strong coordination bonds.[4] The wide array of metal nodes and organic ligands, coupled with various coordination geometries, has facilitated the development of more than 90 000 MOFs to date, a

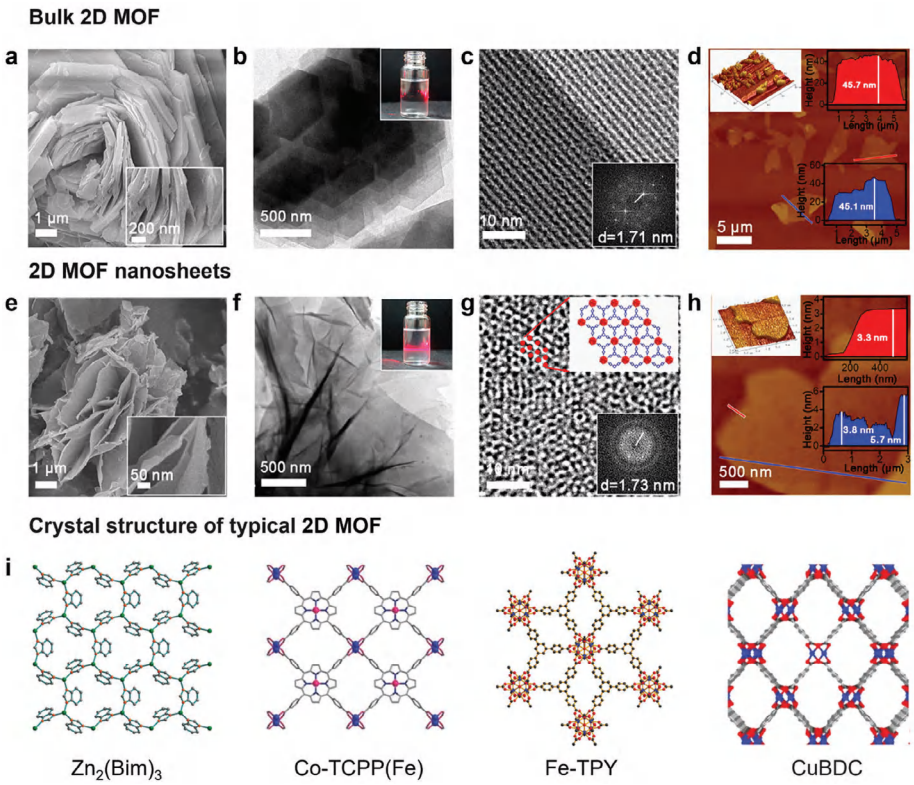

Figure 2. SEM image of a) bulk ZrBTB MOFs and e) 2D ZrBTB MOF nanosheets. TEM image of b) bulk ZrBTB MOFs and f) 2D ZrBTB MOF nanosheets. The inset figure shows the Tyndall light scattering effect of colloidal suspension. e) HR-TEM and FFT images of c) bulk ZrBTB MOFs and g) 2D ZrBTB MOF nanosheets. AFM image and corresponding height profiles of d) bulk ZrBTB MOFs and h) 2D ZrBTB MOF nanosheets. Reproduced with permission from ref.[16] Copyright 2018, American Chemical Society. Crystal structure of typical 2D MOFs, including $Zn_2(Bim)_3$, Co-TCPP(Fe), Fe-TPY, and CuBDC MOFs. Reproduced with permission from ref.[9c,13,25] Copyright 2017, 2016, 2017, Wiley-VCH GmbH & Co. Copyright 2015, Nature.

figure that continues to expand.[11] The surface area of MOFs generally varies from 1000 to 10 000 $m^2\ g^{-1}$, with tunable pore sizes ranging from a few angstroms to ≈10 nm, surpassing the porosity of other typical porous materials like zeolites and porous carbons.[12] The top–down synthesis of 2D MOFs depends on layered bulk MOF particles, often composed of laminar MOF nanosheets that assemble vertically through weak face-to-face interactions or chemically coordinative bonds within their in-plane coordination (**Figure** 2a–d).[13] The synthesized nanosheets generally exhibit a structure analogous to bulk MOFs, featuring similar functional groups, chemical compositions, and coordination environments(Figure 2c,g).[14] In contrast, the bottom–up synthesis of 2D MOFs involves assembling 1D MOFs metal nodes and organic linkers in a specific restricted-growth environment.[14,15] The detailed synthesis methods will be discussed in detail in the next section. Unlike bulk MOFs, 2D MOFs consist of single or few-layer nanosheets, which easily stack tightly through weak face-to-face interactions and roll up to form flower-like structures (Figure 2e,h). Some MOF nanosheets display slight folding and twisting planes due to the size characteristics of ultrathin and flexible nanosheets (Figure 2f).[16] A variety of ultrathin 2D MOFs have been explored so far, such as b-CuBDC,[9c] MnDMS,[17] MOF-5,[18] Ni/Fe-MOF NSs,[19] CoTCPP-py-Cu,[20] 2D Zn-TCPP,[21] Zn/Ni-MOF-2,[22] and CoTCPP-py-Cu,[20] among others (Figure 2i). 2D MOFs combine the advantages of 2D materials (ultrathin thickness, large lateral dimensions, and high surface-to-volume atom ratios) with the unique structure of MOFs (regular nano/microporosity, tunable structures and functions, and high crystallinity).[23] The crystalline architecture of 2D MOF nanosheets offers a significantly exposed surface area and active sites at the atomic scale. The thickness of these nanosheets varies between 0.5 and 1000.0 nm, while their lateral dimensions can range from hundreds of nanometers to several hundred micrometers.[24]

2.2. Properties

The crystalline structure of 2D MOF nanosheets provides a significantly exposed surface area and atomic-level active sites, which can be illustrated by the surface area characteristics of the MOFs.[26] The Brunauer–Emmett–Teller (BET) N_2 adsorption isotherm is a well-established technique for determining pore volume and specific surface area. However, it is important to recognize that in catalytic reactions, the permeability of substrate molecules of varying sizes to access active sites can differ significantly. The "probe molecule" N_2 can easily access nearly all micropores, leading to an overestimation of the actual catalytic surface area. Therefore, even though 3D MOFs may exhibit ultrahigh BET surface areas, they might not provide as many readily accessible active sites compared to their 2D counterparts (2D

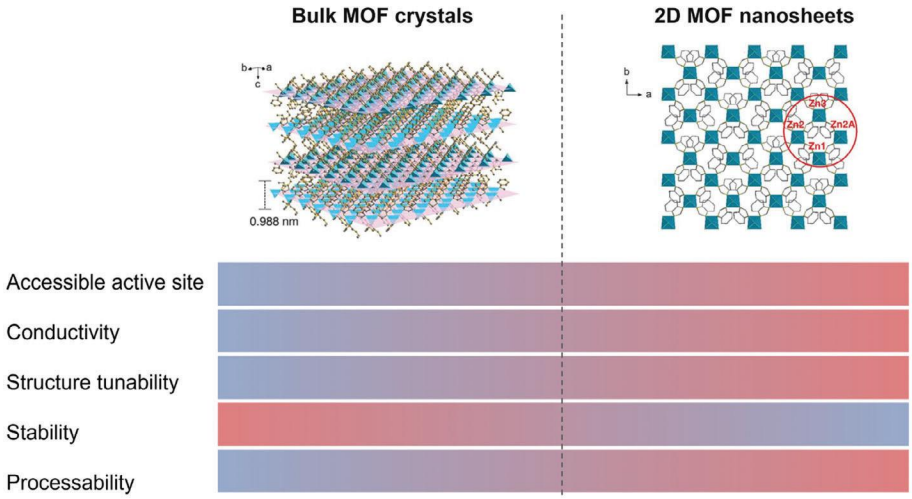

Figure 3. Comparison of bulk MOF crystals and 2D MOF nanosheets. Characteristics of these classes are qualitatively shown; red represents a strong characteristic and blue represents a weak characteristic. Figure of bulk MOF crystals and 2D MOF nanosheets is reproduced with permission from ref.[23] Copyright 2014, Nature.

MOFs). Layered block MOFs suffer from interlayer permeation, resulting in pore blockage.[27] The ultrathin thickness and extensive lateral size of 2D MOF nanosheets guarantee that all active sites are easily accessible for interaction. Thus, transitioning from bulk MOFs to 2D MOF nanosheets generally significantly increases the specific surface area, making active sites more accessible. For example, the BET surface area increased from 504 $m^2\ g^{-1}$ for PCN-641(bulk MOF) to 802 $m^2\ g^{-1}$ for PCN-641-ns (2D MOF nanosheet).[26]

Owing to the benefits such as extensive surface area, readily available active sites, and customizable structures (**Figure 3**), 2D MOFs have emerged as promising candidates for efficient catalysts. First, different from bulk MOFs, 2D MOF nanosheets present a greater number of exposed metal atoms on their surfaces, which serve as active sites for catalysis. The presence of these exposed metal sites, rich in coordinatively unsaturated surface atoms, contributes to enhanced activity.[8] Second, by choosing suitable organic ligands, it is feasible to obtain metal nodes in optimal oxidation states. This is important, as metal species exhibiting elevated oxidation states are particularly advantageous for facilitating oxidation reactions.[28] Thirdly, the ultrathin structure of 2D MOF nanosheets facilitates the creation of vacancies that boost the concentration of charge carriers within the material, ultimately enhancing its conductivity.[29] Fourthly, the considerable porosity and extremely thin nature of 2D MOF nanosheets facilitate the swift mass transfer of reactants and products during catalytic reactions.[30] Lastly, due to the diverse range of metal nodes and organic ligands, a wide variety of 2D MOF nanosheets can be synthesized and investigated as potential catalysts. Due to their superior properties, the catalytic applications of 2D MOF nanosheets have been extensively studied in recent years. The catalytic performance of certain 2D MOF nanosheets is comparable to or even surpasses, that of precious metal-based catalysts.[10c]

So far, while numerous 3D MOF catalysts have been documented for catalytic reactions, there are relatively few studies focusing on 2D MOF nanosheets in this area. This scarcity may be attributed to the limited stability of 2D MOFs when subjected to harsh reaction conditions, including elevated temperatures, potent oxidizing agents, and high pressures.[31] Stability is a key challenge for the application of MOFs, and for ultrathin 2D MOF nanosheets with highly exposed surfaces, stability could be an even bigger issue. To attain enhanced catalytic performance in harsh conditions, it is essential to enhance the stability of 2D MOFs. A key element in improving the stability of 2D MOFs is strengthening the interactions between metal nodes and organic ligands.[32] For instance, enhancing the strong electrostatic interactions between highly acidic metal ions and highly basic ligands can play a significant role in this process.[32] By using high-valence metal ions (like Zr^{4+}) to bond with organic ligands and construct highly connected MOFs, water stability can be significantly improved.[33] The strong Zr—O bonds and numerous chelating carboxylate linkages to the Zr_6 clusters and metal clusters with high connectivity can protect the metal cluster structurally, ensuring the stability of Zr-MOFs in demanding chemical environments.[34] Studies on the stability of 2D MOFs have been limited so far. Research has demonstrated that ultrathin Zr-MF-ZrBTB nanosheets with nanoscale thickness maintain stability at temperatures as high as 494 °C in an air environment, comparable to that of bulk ST-ZrBTB.[16] Although certain studies have concentrated on the thermal stability of 2D MOF nanosheets, there is a notable lack of systematic research regarding their stability under other extreme reaction conditions, including strong acidic and basic electrolytes, highly polar solvents, elevated temperatures, oxidative or reductive gases, and potent oxidants produced during exposure to visible light. The environmental stability of 2D MOFs needs to be carefully considered in future research endeavors.

Shaping MOFs into macroscopic or mesoscopic forms with hierarchical pore structures can effectively enhance their applicability in industrial scenarios.[35] However, due to their inherent lack of fluidity, bulk MOF crystals and nanocrystals suffer from poor processability. The unsatisfied processability poses a significant challenge for scaling up the fabrication of MOF-based devices

such as membranes and electronic devices, thus limiting industrial applications.[36] The direct application of micro/nano MOF powders encounters several technical hurdles, including challenges related to improper handling, limitations in mass transfer, dust generation, and unnecessary pressure drops within packed beds. The difficulties associated with the poor processability of bulk MOFs can be traced back to their insolubility, which arises from a rigid, crystalline network structure. Several strategies have been proposed to mitigate these challenges, such as post-synthetic modification of specific functional groups, enabling good dispersion and stability of MOF particles in solvents.[37] Nonetheless, this approach requires careful functionalization of MOF particles, as the incorporation of organic molecules may lead to the introduction of inactive substances. This can result in the clogging of MOF pores and negatively impact the physicochemical properties of the modified MOFs. 2D MOF nanosheets featuring high aspect ratios, precisely adjustable thicknesses ranging from monolayers to multilayers, and easier access to active sites often exhibit distinct physicochemical properties compared to bulk counterparts. Early studies on 2D MOF nanosheets primarily focused on synthesis, initially confirming the nanometer size and dispersity of 2D MOFs through light scattering. The adsorption of solvent molecules at specific locations on 2D MOF nanosheets can help stabilize them, allowing the clear observation of the Tyndall effect in colloidal suspensions of 2D MOF nanosheets.[23] The interlayer interactions of MOFs can be compensated by judiciously selecting solvents to enhance the interaction between MOF nanosheets and solvents. Therefore, the aggregation of MOF nanosheets can be avoided, thus stabilizing the resulting nanosheets. In 2021, Yuan et al.[38] indicated that the adsorption energies of N, N-dimethylformamide (DMF), H_2O, and acetone on NUS-8 MOF nanosheets were greater than the interlayer interactions of NUS-8, with values of −158.24, −215.22, and −140.16 kJ mol^{-1}, respectively, in contrast to −84.39 kJ mol^{-1} for the interlayer interactions. The enhanced interactions between the solvents and NUS-8 nanosheets effectively inhibited the stacking of the nanosheets, thereby providing significant stabilization. Conversely, weaker interactions between the solvents and the nanosheets result in considerable aggregation. The interactions between individual nanosheets and between the nanosheets and solvents are primarily governed by van der Waals forces. As a result, 2D MOF nanosheets progressively develop a colloidal state within the liquid medium, forming a weak, non-covalently bonded colloidal network structure that conforms to the shape of the container.[39] Overall, suspensions composed of 2D MOF nanosheets demonstrate better solution processability compared to bulk MOFs. Therefore, utilizing 2D MOF nanosheets as building blocks to create binderless monolithic sheets, aerogels, dry gels, or even uniform membranes with adjustable thickness is promising, benefiting their environmental applications.

3. Synthesis Methods

A variety of techniques have been established for the synthesis of 2D MOF nanosheets, each designed to meet specific application requirements. These synthesis methods can generally be classified into two main categories: i) top–down methods that involve overcoming weak interlayer interactions (such as van der Waals) through mechanical, ultrasonic, or chemical means to exfoliate bulk materials, and ii) bottom–up methods that rely on controlling the growth kinetics of MOFs crystals in different crystallographic directions. The representative methods for synthesizing 2D MOF nanosheets are detailed in the following sections and are briefly summarized in **Table 1**.

3.1. Top–Down Method

The advancement of layered MOFs has largely been influenced by the solution-based synthesis techniques used for more established van der Waals materials, such as graphene, MoS_2, and other transition metal chalcogenides, owing to their structural similarities. Exfoliation is a widely used and effective method for generating MOF nanosheets. Layered bulk MOFs are held together by weak interactions, such as hydrogen bonding and van der Waals forces. These materials can be processed into 2D MOF nanosheets or nanoribbons with desired dimensions through exfoliation methods, which encompass both physical and chemical exfoliation techniques.[7c] The crucial step in the synthesis of 2D MOF nanostructures involves breaking the relatively weak interactions between adjacent layers of bulk MOFs, either through the application of external forces or by increasing the interlayer distance via molecular insertion. Single-layer 2D MOF nanomaterials can be achieved using a range of physical exfoliation techniques, which include ball milling, shaking, mechanical force, ultrasonication, and freeze–thaw exfoliation.[23,40] Ultrasonication in specific solvents has been proven to be the most common and practical method for producing nanosheets. Utilizing ultrasonic energy facilitates the breaking of interlayer bonds, thereby improving the efficiency of the exfoliation process (**Figure 4a**). The choice of solvent significantly affects the efficiency of the physical exfoliation process as different solvents have varying impacts on exfoliation efficiency.[23] Proper surface tension, suitable viscosity, and good wetting properties are also the key solvent characteristics for achieving high exfoliation rates. Examples of typical solvents include methanol, ethanol, isopropanol, and DMF.[41] Based on selecting the appropriate solvent, rough control over the thickness, lateral size, and suspension concentration of MOF nanosheets can be achieved by controlling ultrasonic frequency, energy density, amplitude, power, and duration.

Chemical delamination primarily employs chemical reactions to overcome interactions between block-like MOF precursor layers, which refers to unstable covalent or coordination bonds, while preserving the in-plane coordinating bonds. By incorporating chemically labile out-of-plane ligands between the layers of MOF structures, it is feasible to transform layered MOFs into pseudo-pillared MOFs. This modification increases their susceptibility to exfoliation by facilitating the cleavage of the out-of-plane ligands. For instance, Ding et al.[43] presented an efficient method for generating 2D MOF nanosheets derived from intrinsically layered porphyrinic MOFs. This approach incorporated both crystal intercalation and a chemical exfoliation process (Figure 4b). They initially included 4,4′-dipyridyl disulfide (DPDS) into layered MOF crystals through coordination with the metal nodes. Then, they chemically reduced the disulfide bonds in DPDS

Table 1. Different methods for synthesizing 2D MOF nanosheets.

Category	Synthesis method	Principle	Advantages	Disadvantages
Top–down methods	Physical exfoliation	Applying external forces, including ball milling, shaking, mechanical force, ultrasonication, or freeze–thaw exfoliation, to break the relatively weak interactions between adjacent layers of bulk MOFs.	Mild conditions, high-quality nanosheets, scalable.	Large distribution in size, and thickness, low yield, time-consuming.
	Chemical delamination	Using chemical reactions to break the interactions between bulk MOF layers.	High yield, rapid synthesis.	Additional chemical reagents, presence of defects.
Bottom–up methods	Interface oriented growth	Restricting the reaction region of metal ions and organic linkers into the interface between two phases.	Easy to customize, large size, high-quality nanosheets, less defect.	Difficult to transfer.
	Modulator-assisted growth	The modulator competes axially with the organic ligand to ensure the anisotropic growth of the 2D MOF nanosheet.	Prevent the aggregation of MOF nanosheets, uniform size, scalable.	Additional chemical reagents, presence of defects.
	Confined growth	Using confined microreactors induced by microemulsions or nanomaterials to inhibit the out-of-plane growth of MOF nanosheets and promote mass/heat transfer.	High yield, rapid synthesis, scalable.	Aggregation of synthesized 2D MOFs, complex synthesis device.

using trimethylphosphine (TMP), leading to reduced interlayer interactions and the formation of thin MOF nanosheets (≈1 nm thick).

It is worth noting that, in this top–down exfoliation process, coordination bonds within the MOFs plane may still be disrupted. This disruption often results in low yield, uneven distribution, and subpar quality of 2D MOFs. Nevertheless, exfoliation continues to be one of the most widely used methods for synthesizing 2D MOFs due to its simplicity and compatibility with a range of bulk MOF types.

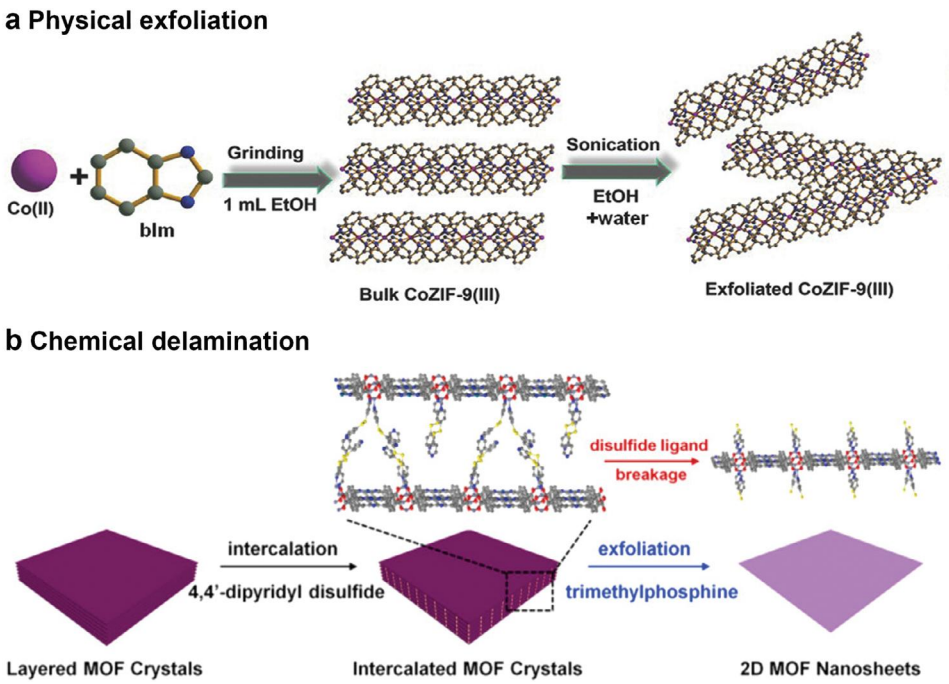

Figure 4. a) The schematic diagram illustrating the synthesis procedure of CoZIF-9 (III) nanosheets via the sonication method in a mixture of EtOH and water. Reproduced with permission from ref.[42] Copyright 2018, Wiley-VCH GmbH & Co. b) Schematic of the 4,4′-dipyridyl disulfide intercalation process, followed by exfoliation through disulfide ligand cleavage. Reproduced with permission from ref.[43] Copyright 2017, American Chemical Society.

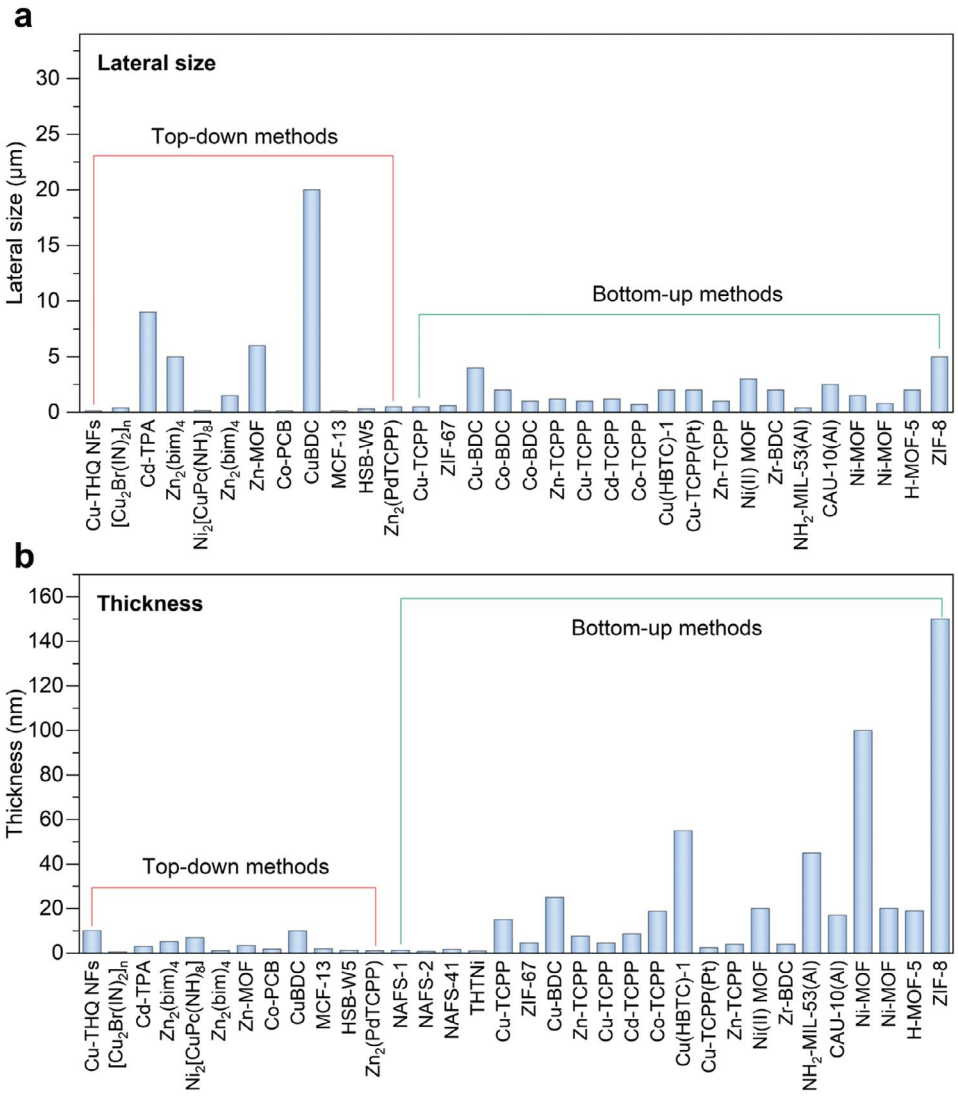

Figure 5. a) Lateral size of typical 2D MOFs from refs.[9c,14,18,23,41,43,44], b) Thickness of typical 2D MOFs from refs.[9c,14,18,20,23,41,43,44b–k,n–v,45]

3.2. Bottom–Up Method

In general, a critical challenge in producing MOF nanosheets through bottom–up approaches is to prevent out-of-plane coordination or growth. Based on this principle, bottom–up methods can be categorized into interface-oriented growth (including solid–air, liquid–air, and liquid–liquid), modulator-assisted growth (typically involving capping solvents and surfactants), or confined growth. Generally, 2D organic ligands, particularly those with planar coordination sites aligned parallel to the sheet plane, are favored for the growth of nanosheets. The various growth mechanisms lead to significant differences in the lateral dimensions and thickness of MOF nanosheets, which can range from single-layer to a few layers, resulting in varying yields of nanosheets. Generally speaking, compared with the top–down method, the 2D MOF prepared by the bottom–up method is generally smaller and thicker than the 2D MOF prepared by the top–down method (**Figure 5**).

By employing interfacial growth techniques, single-layer MOF nanosheets with considerably larger lateral dimensions can be generated. The chemical properties and structure of these nanosheets can be customized through careful ligand design and manipulation of synthesis parameters, including reagent concentration, substrate selection, and solvent type. In the case of solid–gas interfacial growth, coordination reactions take place on a pristine surface, where metal sources and organic ligands are deposited successively.[46] Unfortunately, there are no existing reports on the successful removal of nanosheets from the substrate surface to obtain individual nanosheets. Preserving crystallinity while avoiding the introduction of additional defects is a critical challenge during the peeling and transfer processes. In liquid–liquid interfacial growth, two immiscible liquid systems are utilized, each containing metal ions and bridging ligands. The

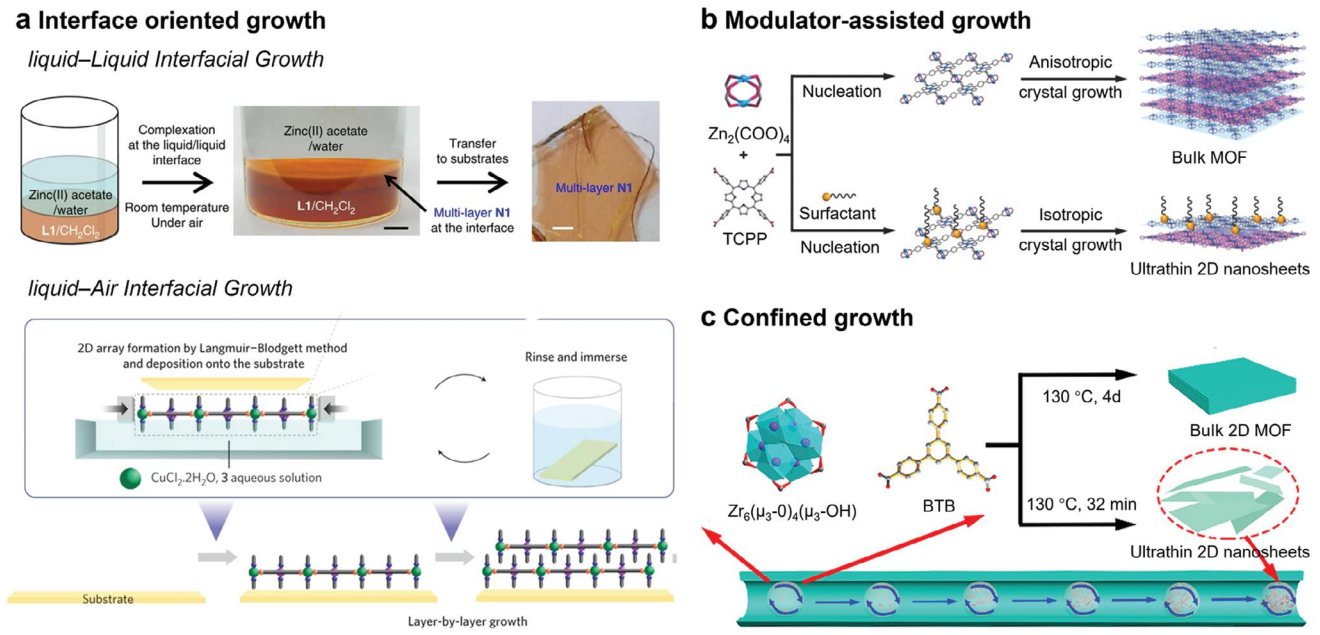

Figure 6. a) Top: The schematic diagram illustrating the liquid–liquid interfacial growth of the N1 MOF nanosheet and the subsequent transfer. Scale bar in the middle and right: 5 and 1 mm. Reproduced with permission from ref.[15a] Copyright 2015, Nature. Bottom: Schematic of liquid–air interfacial growth of NAFS-1 MOF nanosheets. Reproduced with permission from ref.[20] Copyright 2010, Nature. b) The traditional isotropic growth of the bulk MOF crystal (top) and surfactant-assisted anisotropic growth of 2D MOF nanosheets (bottom). Reproduced with permission from ref.[14] Copyright 2015, Wiley-VCH GmbH & Co. c) Schematic diagram showing the solvothermal method (top) and microdroplet confined synthesis of the ZrBTB (bottom). Reproduced with permission from ref.[16] Copyright 2017, American Chemical Society.

reaction occurs at the interface between these two liquid phases, typically resulting in nanosheet thicknesses in the range of hundreds of nanometers (**Figure 6a**).[15a] Liquid–gas interfacial growth is one of the most commonly employed methods for generating single-layer and few-layer MOF nanosheets. This method's popularity primarily stems from its simplicity, ease of nanosheet transfer, and the advantages of a tightly packed structure facilitated by the utilization of a Langmuir–Blodgett trough.[20]

The solvent thermal synthesis approach has been extensively utilized for producing 3D MOF nanoparticles and bulk-layered MOFs. However, the direct synthesis of ultrathin MOF nanosheets continues to pose a considerable challenge due to their elevated surface energy. When fabricating simple MOF nanosheets, this strategy usually incorporates modulators or surfactants to inhibit out-of-plane growth and the formation of stacks. These modulators, often referred to as capping agents, compete with organic ligands for coordination in the axial direction, thereby promoting the anisotropic growth of MOF nanosheet crystals.[47] Because modulators typically lack multiple binding sites or the ability to connect metal nodes, they effectively halt the growth of MOFs. Various structure-modulating agents have been employed, including ammonia, pyridine, formic acid, gluconate, acetic acid, and solvent mixtures such as water.[48] Modulators, due to their competitive binding characteristics with organic linker molecules, can also lead to the introduction of additional defects in the form of mesoporosity within MOF nanosheets. Furthermore, the successful application of surfactants in shaping the morphology of nanomaterials can similarly be utilized in the synthesis of 2D MOFs.[14] This is accomplished through the preferential adsorption of surfactants onto specific crystal planes of certain MOFs, which restricts their growth and consequently limits the out-of-plane growth direction in the case of 2D MOFs (Figure 6b).[14] Surfactants such as sodium dodecyl sulfate (SDS), cetyltrimethylammonium bromide (CTAB), and polyvinylpyrrolidone (PVP) have been widely used as structure-directing agents in the manufacture of MOF nanosheets.[14,49] It is worth noting that the surfactant can also be adsorbed on the surface of the nanosheet, which helps to reduce surface energy and prevent stacking.

Microemulsions or closed micro-reactors created by nanomaterials can be employed to inhibit the lateral growth of MOF nanosheets while enhancing mass and heat transfer. Mechanically manipulating well-dispersed microemulsion droplets in equal numbers of reaction regions generates uniform high-yield nanosheets. A novel continuous bottom–up approach is introduced by Wang et al.[16] for producing ultrathin (≈3 nm) 2D MOF nanosheets with high crystallinity (Figure 6c). In contrast to traditional solvothermal synthesis techniques employed for 2D MOFs, the microdroplet flow system utilizes dynamic mixing reactions. This approach, which is defined by both diffusion and forced convection, effectively restricts the longitudinal growth of stacked 2D ZrBTB structures. As a result, ultrathin and well-separated 2D ZrBTB nanosheets, referred to as MF-ZrBTB (with "MF" standing for "microdroplet flow reaction"), were successfully synthesized. These nanosheets exhibited lateral dimensions ranging from 1 to 5 μm and had an approximate thickness of 3 nm, resulting in an impressive space–time yield (STY) of 385.03 kg m^{-3} per day. Confined growth in closed systems represents a promising approach for producing MOF

Table 2. Adsorption capacity and adsorption mechanism of representative 2D MOF.

2D MOF	Pollutants	Adsorption capacity	Adsorption mechanism	Refs.
Zn(Bim)(OAc)	Pb(II) and Cu(II)	253.8 and 335.57 mg g^{-1}	Coordination interaction of hydroxyl and imino groups	[50]
Cu-MOF	Pb^{2+}	738.65 mg g^{-1}	Electrostatic interaction, coordination interaction between carboxyl groups and Pb^{2+}	[51]
HSB-W15-NS	Fe^{3+}	250.81 mg g^{-1}	Coordination interaction of free amino, pyridyl, and uncoordinated carbonyl groups	[52]
CoCNSP	Hg(II), U(VI), Pb(II), and Cu(II)	716, 661, 534, and 325 mg g^{-1}	Inner-sphere coordination between sulfur species and heavy metals	[53]
2D-NCS	$HgCl_2$	1698 mg g^{-1}	Cation-π and Hg...S interactions	[44d]
kgd-Zn@MF	CIP	239.2 mg g^{-1}	Electrostatic interaction, hydrophobic interaction, π–π stacking, and hydrogen bonding	[54]
	oils	5077–13 786 wt%	n.a.	
ZnO@CuBDC_A1	1-heptanethiol	23.9 mg g^{-1}	Coordination interaction between Cu^{2+} and 1-heptanethiol	[55]
ZIF-8/NH_2-MIL-53(Al)	DOX, TET, OTC, and CTC	561, 533, 526 and 578 mg g^{-1}	Hydrogen-bonding interaction, chemisorption, and π–π interaction/stacking	[56]
Zr-BTB-H4TBAPy	RhB and MB	238 and 124 mg g^{-1}	Electrostatic interaction	[57]
Cu(II)-5N_3IP	MB, RhB, MO, and CR	n.a.	Electronic interactions, π–π interactions, and hydrogen bonds	[58]
UPC-28	RhB and MB	n.a.	Electrostatic interaction, size-selective effect, and π–π interactions	[59]
BIPT-1·3H_2O·DMF	MB	26 mg g^{-1}	Electrostatic interaction	[60]
MOF 1	NR, BR, and MO	n.a.	Size-exclusive effect	[61]

DOX, Doxycycline; TET, Tetracycline; OTC, Oxytetracycline; CTC, Chlortetracycline; MB, Methylene blue; RhB, Rhodamine B; MO, Methyl orange; CR, Congo red; NR, Neutral red; BR, Basic red 2; CIP, Ciprofloxacin.

nanosheets with a high aspect ratio. These relatively new methods are conducive to enhancing productivity without the use of environmentally harmful substances, thus eliminating negative implications for further applications.

4. Environmental Applications

4.1. Contaminant Adsorption

4.1.1. Adsorption of Heavy Metal Ions

In comparison to 3D porous adsorbents, 2D MOF nanosheets retain the structural attributes of MOFs, including a periodic arrangement with specifically engineered adsorption sites. Additionally, they address the limitations associated with 3D porous materials, particularly the restricted accessibility to active sites. 2D MOF nanosheets fully utilize the adsorption sites, providing excellent adsorption performance. As a result, 2D MOF nanosheets are anticipated to be excellent candidates for attaining a high adsorption capacity for pollutants, particularly heavy metal ions (**Table 2**). For example, due to their exceptionally thin structure and a high degree of exposed active sites, the synthesized ultrathin Zn(Bim)(OAc) nanosheets demonstrated impressive adsorption capacities of 253.8 mg g^{-1} for Pb(II) and 335.57 mg g^{-1} for Cu(II). These values significantly surpassed the adsorptive uptake observed in their bulk-type MOF counterparts, which showed capacities of 198.02 g^{-1} for Cu(II) and 159.23 mg for Pb(II) (**Figure 7a–c**).[50] Simultaneously, the saturation process occurred swiftly, taking just 30 min for Cu(II) and 90 min for Pb(II). The adsorption capacity of 2D Cu-MOF nanosheets for Pb^{2+} could attain as much as 738.65 mg g^{-1}, surpassing the capacity of 3D Cu-MOFs (509.56 mg g^{-1}). This enhanced performance can be attributed to several factors inherent to the unique structure of the nanosheets. First, the ultrathin nature of the nanosheets provides a greater exposed surface area, which facilitates an increased interaction with the target metal ions. Additionally, the intrinsic cavity formations within the nanosheet architecture create abundant sites for adsorption, effectively enhancing the material's engagement with metal ions. Furthermore, the 2D morphology allows for greater accessibility to the active sites, minimizing diffusion limitations that are often associated with bulkier 3D structures. This unique combination of high surface area, accessible active sites, and effective ion capture mechanisms underscores the superiority of 2D MOF nanosheets in environmental applications, particularly in the efficient removal of heavy metal contaminants from aqueous solutions.[51]

Electrostatic attraction and coordination interactions play essential roles in influencing the adsorption of heavy metal ions. The electrostatic interaction can be confirmed by adsorption results under different pH conditions and Zeta potential measurements (Figure 7d).[51] As the pH of the solution rises, the potential of the MOF nanosheets experiences a rapid decline. In contrast, the efficiency of heavy metal removal exhibits an opposite trend, significantly increasing as the solution pH increases (Figure 7e). At lower pH levels, the adsorption sites become protonated and are occupied by H^+ ions. High concentrations of H^+ can compete with heavy metal ions for the active sites on the surface of the MOF nanosheets, potentially hindering adsorption. However, as the pH of the solution rises, the deprotonation of the adsorbent results in a reduction of the MOF nanosheets' potential. This decrease alleviates the competitive in-

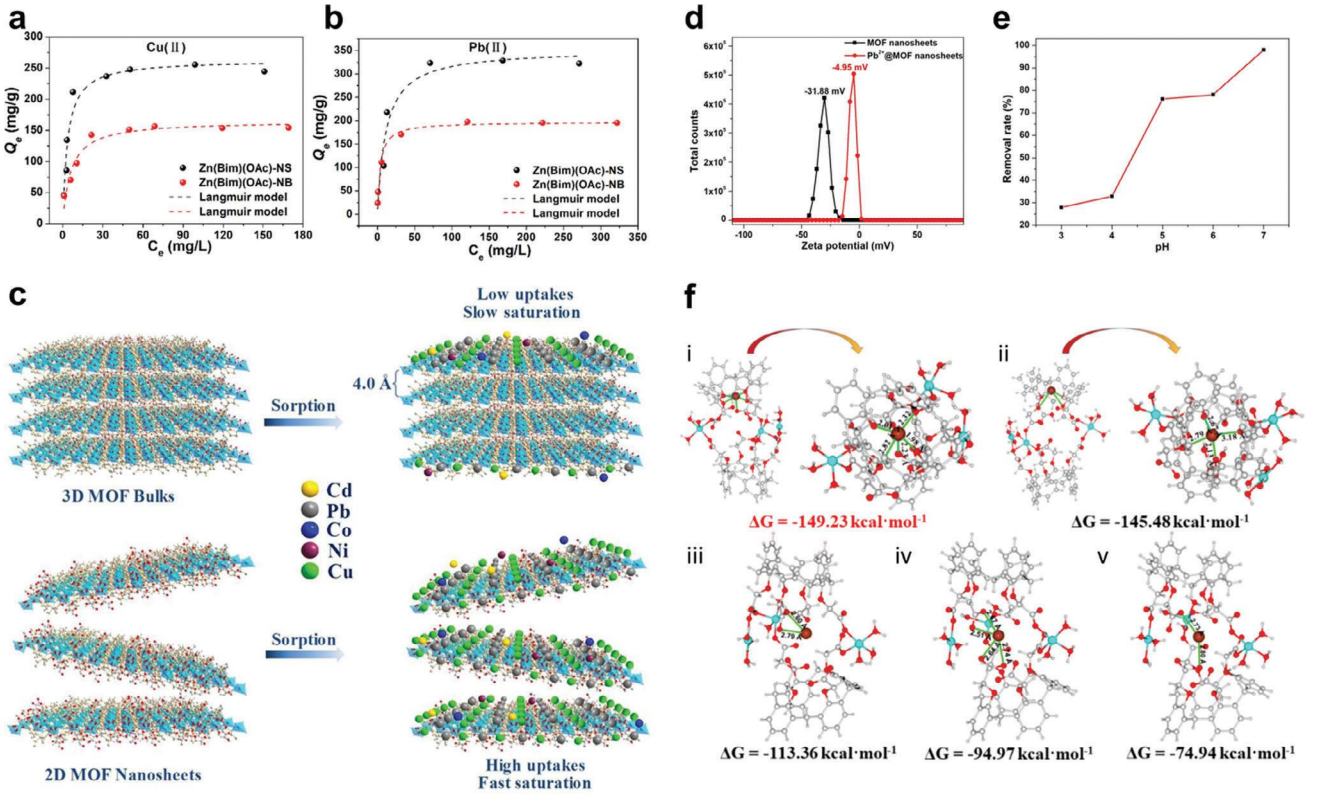

Figure 7. Adsorption isotherms of a) Cu(II) and b) Pb(II) on Zn(Bim)(OAc)-NS and Zn(Bim)(OAc)-NB; (Adsorbents dose: 200 mg L^{-1}; adsorption time: 1.5 h, initial pH: 5.5 ± 0.1, temperature: 25 °C). c) Schematic diagram illustrating the potential combination mode of Pb(II) and Cu(II) on Zn(Bim)(OAc)-NB and Zn(Bim)(OAc)-NS. Reproduced with permission from ref.[50] Copyright 2020, Elsevier. d) Zeta potentials of MOF nanosheets and Pb^{2+}@MOF nanosheets. e) Effect of pH on Pb^{2+} adsorption by MOF nanosheets. f) Optimized cage-like cavity in Cu-MOFs via DFT simulation and identification of potential interaction types with Pb^{2+} during the adsorption process. Color codes: cyan, Cu; brown, Pb; red, O; gray, C; light gray, H. Reproduced with permission from ref.[51] Copyright 2023, Royal Society of Chemistry.

fluence of H^+, thereby facilitating enhanced adsorption. Initially, the primary driving force for adsorption is electrostatic attraction, which exhibits lower selectivity before the pollutant molecules come into proximity. Once in close contact, the dominant interaction shifts to coordination interactions, which display higher selectivity. In the case of 2D MOF nanosheets, the exposed surface area creates additional opportunities for close contact and interaction with pollutant molecules. This enhances the coordination interactions between the functional groups present on the MOF surface, such as amino, carboxyl, and hydroxyl groups, and metal ions. Consequently, this significantly improves the adsorption selectivity of the 2D MOF nanosheets (Figure 7f).[51] For 3D MOF adsorbents, the adsorption sites that are embedded within the framework face challenges in establishing close contact with pollutant molecules. As a result, the adsorption process is primarily influenced by the adsorption driving force and electrostatic attraction for the majority of the time. Therefore, insufficient closeness in contact leads to generally lower adsorption selectivity in 3D MOFs compared to 2D MOF nanosheets.

In general, 2D MOFs can offer an attractive platform to address issues such as improper distribution or burial of functional groups in other heavy metal ion adsorption materials. The highly adjustable structure and properties of MOFs provide numerous possibilities for optimizing performance further. For example, Sun et al.[51] introduced 2D MOF nanosheets featuring cavity structures, utilizing the carefully chosen pro-ligand 25, 26, 28-tetrakis[(carboxyl)m]calix[4]arene. The presence of highly accessible and uncoordinated oxygen-containing functional groups, such as carboxyl and ether groups, within the cage-like cavities provides effective adsorption sites. Additionally, these cavities within MOF nanosheets function as containers for pollutants, resulting in outstanding adsorption performance for^{2+} ions in the synthesized Cu-MOF nanosheets. In addition to changes in the connectivity structure, the strategic introduction of other highly selective functional groups is expected to further enhance adsorption selectivity. For instance, following the hard and soft acids and bases (HSAB) principle, thio groups (S^{2-}) as soft Lewis acids can be advantageous for selective interaction with late-transition heavy metals, particularly Hg^{2+}.[41,44d] Other strategies such as defect engineering, post-modification, and nano-composites also hold promise for enhancing the adsorption performance of 2D MOF nanosheets. However, research in this area remains very limited.

The 2D MOFs benefit from the periodic arrangement of chelating groups, enhancing their ability to bind metals, and resulting in unexpectedly high adsorption performance. This periodic structure of MOFs supports systematic enhancements and investigations into the correlation between structure and func-

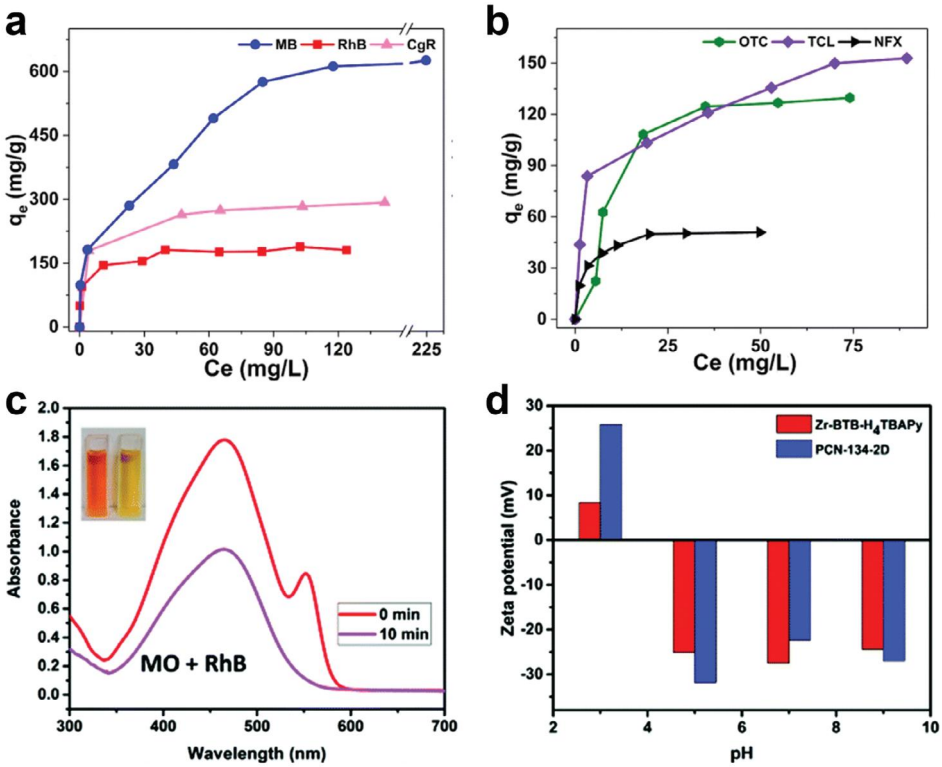

Figure 8. Adsorption isotherms of Cu-TCPP for a) different dyes and b) antibiotics. Reproduced with permission from ref.[62] Copyright 2023, Springer Nature. c) The UV–vis spectra and images of MO and RhB mixed dye solutions before and after adsorption by Zr-BTB-H_4TBAPy. d) The zeta potentials of Zr-BTB-H_4TBAPy and PCN-134-2D at different pH. Reproduced with permission from ref.[44e] Copyright 2021, Royal Society of Chemistry.

tion. However, from a practical standpoint, many still face issues of insufficient hydrolytic stability, particularly under harsh water conditions. For instance, Zn(Bim)(OAc)-NS has shown a tendency to dissolve at pH levels below 4.[50] Furthermore, current research exhibits a significant gap in addressing the cyclic stability of 2D MOF materials, as well as the desorption of heavy metal ions and the recycling processes associated with these materials.

4.1.2. Adsorption of Organic Contaminants

2D MOF nanosheets also serve as effective adsorbents for eliminating organic contaminants, including dyes, oils, and pharmaceutical residues. Their remarkable adsorption performance can be attributed to the abundant active sites on their surface and their substantial surface area. Based on their strong adsorption capacity for various organic dye molecules, including rhodamine B (RhB), methylene blue (MB), congo red (CR), methyl orange (MO), bromophenol blue (BB), and acid fuchsin (AF) (Table 2). The maximum adsorption capacity of 2D MOF nanosheets for MB could reach as high as 625.0 mg g^{-1} (**Figure 8a**), making them comparable to adsorbents based on graphene.[62] The process of dye adsorption is primarily thought to be driven by electrostatic interactions and van der Waals forces. When 2D MOF nanosheets carry a negative charge, the adsorption rate for cationic dyes (such as RhB) is faster than for anionic dyes (like MO), highlighting the importance of electrostatic attraction. As a result, nanosheets can selectively capture cationic dyes from a mixture containing both anionic and cationic dyes in solution, making them suitable for dye separation (Figure 8c,d).[44e] Furthermore, the physical dimensions of the dye molecules themselves are crucial in dictating adsorption behavior; for instance, smaller molecules like MB tend to be adsorbed more readily than their larger counterparts, such as RhB, due to less steric hindrance and more favorable diffusion dynamics through the nanosheet structure.[58] Additionally, the adsorption process is likely enhanced by other weak interactions, including π–π stacking between the aromatic rings of the dye molecules and the organic linkers within the MOF framework, which can further stabilize the dye-MOF interaction and augment overall adsorption capacity.[59] These combined effects illustrate how the unique structural and chemical properties of 2D MOF nanosheets culminate in their superior performance as adsorbents in the removal of dyes and other organic contaminants from wastewater.

Coating 2D MOF nanosheets on the substrate surface to construct MOF composite materials effectively removes insoluble oils in water while avoiding potential recovery difficulties and secondary pollution. Hydrophobic interactions are mainly responsible for the oil and organic solvent removal by 2D MOFs nanosheet-based adsorbent materials. For instance, Gai et al.[54] introduced the integration of a kgd topological MOF (kgd-Zn) onto melamine foam (MF) to produce a 3D porous material known as kgd-Zn@MF. The MOF shell acted as a barrier, inhibiting water molecules from penetrating the pores of the foam. In contrast, oil droplets can easily penetrate both kgd-Zn@MF and MF. The water contact angle rose dramatically from 0° of MF

to 130° of kgd-Zn@MF, demonstrating significant hydrophobic properties. This hybrid material displayed an impressive absorption capacity and recyclability for solvents and oils, ranging from 5077 to 13 786 wt%, surpassing many commercial and previously reported high-performance adsorbents.

Removing residual antibiotics from water is of great significance, yet it remains a significant challenge in water purification. Adsorbents based on 2D MOFs demonstrate excellent adsorption performance for various antibiotics, including oxytetracycline (OTC), tetracycline (TET), chlortetracycline (CTC), doxycycline (DOX), norfloxacin, and ciprofloxacin (CIP). For instance, the adsorption capacity of 2D Cu-TCPP for tetracycline can reach 150 mg g^{-1} (Figure 8b).[62] The adsorption process is primarily determined by electrostatic interactions, π–π stacking, hydrophobic interactions, and hydrogen bonding. Electrostatic and hydrophobic interactions are influenced by the solution's pH. Different pH values can lead to varied protonation–deprotonation processes of CIP molecules, resulting in different configurations. Research by Gai et al. explored the impact of pH on the adsorption capacity of kgd-Zn for CIP.[54] As the pH increased from 2.0 to 3.0, the absorption of CIP increased, but a significant decrease was observed when the pH exceeded 7.0. The Zeta potential indicated that at pH below 2.53, the kgd-Zn particle surface was positively charged, while above 2.53, the surface became negatively charged. Within the pH range of 6.0 to 9.0, the CIP solution contains a significant amount of cationic or zwitterionic compounds. The negatively charged kgd-Zn adsorbent enhances the adsorption of CIP through both electrostatic and hydrophobic interactions. However, when the pH drops below 6.0, the increased protonation of CIP diminishes hydrophobic interactions by eliminating zwitterionic forms, which impedes their attachment to kgd-Zn. Conversely, at pH levels above 9.0, the rise in anionic CIP species causes greater electrostatic repulsion, resulting in a reduced adsorption capacity. Additionally, in MOFs that incorporate benzene or pyridine rings, π–π interactions between the MOF structure and antibiotic molecules significantly contribute to the adsorption process, as evidenced by infrared spectroscopy analysis. Moreover, 2D MOF nanosheets typically have highly exposed hydrophilic groups like carboxyl and amino groups, facilitating hydrogen bonding with antibiotic molecules and thereby enhancing the adsorption process.

4.2. Photocatalytic Degradation

The increased light penetration and greater exposure of catalytic active sites position 2D MOF nanosheets as highly promising photocatalysts in environmental applications. The photocatalytic process can be broken down into three key stages: light absorption, the separation and transport of photoinduced charge carriers, and surface reduction or oxidation reactions. Photogenerated electrons and holes on the photocatalyst surface can react with dissolved oxygen and water to form reactive oxygen species (ROS), effectively degrading or mineralizing organic pollutants. Light absorption is essential for the entire photocatalytic process, necessitating that materials possess a wide range of light absorption capabilities, spanning from ultraviolet to visible light. When the energy of the incoming photons exceeds the material's bandgap (hv≥Eg), the material can efficiently absorb a significant portion of photons present in the solar spectrum. Due to the high electron density, aromatic carboxylate ligands exhibit strong ultraviolet absorption peaks ≈250 nm. A practical approach involves tailoring appropriate bandgaps by altering functional groups on aromatic ligands, such as $-NH_2$, incorporating various dye chromophores (such as porphyrin or boron dipyrromethene), or by modifying metal ions and metal oxide clusters.[63] Following light excitation, the strong binding and rigid conjugation between organic ligands and metal nodes in MOFs facilitate the separation and diffusion of photo-induced carriers on the catalyst surface, enabling the transfer of electrons from the ligands to the metal nodes.[64]

The low photocatalytic efficiency of 3D bulk MOFs is still hindered by the limited exposed catalytic surface area and slow separation of photoinduced electron–hole pairs. Minimizing the thickness of MOF materials to the atomic scale can effectively reduce electron–hole recombination and improve charge conversion efficiency, thereby combining the advantages of 2D materials and MOFs in photocatalytic applications. 2D MOF nanosheets have distinguished themselves in the field of photocatalysis due to their multifaceted capabilities, which encompass not only efficient mass transfer pathways and robust electron conduction but also a substantial abundance of catalytically active sites and light-absorbing centers. The unique layered architecture of these nanosheets facilitates the rapid transportation of molecules and ions, significantly reducing the resistance associated with mass transfer, a critical factor in enhancing the reaction rates during photocatalytic processes. Moreover, the inherent electronic characteristics of 2D MOF nanosheets promote exceptional electron conduction, enabling effective charge separation and transfer in photocatalytic or electrochemical reactions. For example, the 2D zinc(II) MOF exhibited notable photocatalytic prowess in degrading organic dyes, surpassing other MOFs by achieving degradation rates of 98.5% for RhB and 83.8% for MO in 120 min due to its potent generation of $\cdot O_2^-$.[65] 2D MOF nanosheets exhibit not only effective mass transfer pathways and electron conduction but also a significant abundance of catalytically active sites and light-absorbing centers. The high density of catalytically active sites provides ample reactive venues for the degradation of hazardous substances by reducing the diffusion distances for both products and reactants. Additionally, the presence of light-absorbing centers allows these nanosheets to effectively harness solar energy. As a result, the performance of vertically aligned 2D Ni-MOF nanosheet arrays supported on nickel foam exceeded that of 3 bulk Ni-MOF materials, achieving an outstanding mineralization of 86.6% and successfully removing 98.1% of ethyl acetate.[66] Collectively, these attributes underscore the remarkable potential of 2D MOF nanosheets in the advancement of innovative water treatment technologies aimed at addressing the pressing environmental challenges posed by water pollution. However, stability remains a key challenge, particularly for ultrathin 2D MOF nanosheets, indicating careful consideration is necessary for practical water treatment applications.

By harnessing the synergistic effects arising from the combination of heterogeneous materials, researchers can substantially broaden the absorption spectrum of visible light and enhance the effective separation of photogenerated charge carriers within photocatalytic systems based on 2D MOFs. This deliberate combination of different materials enables the formation of

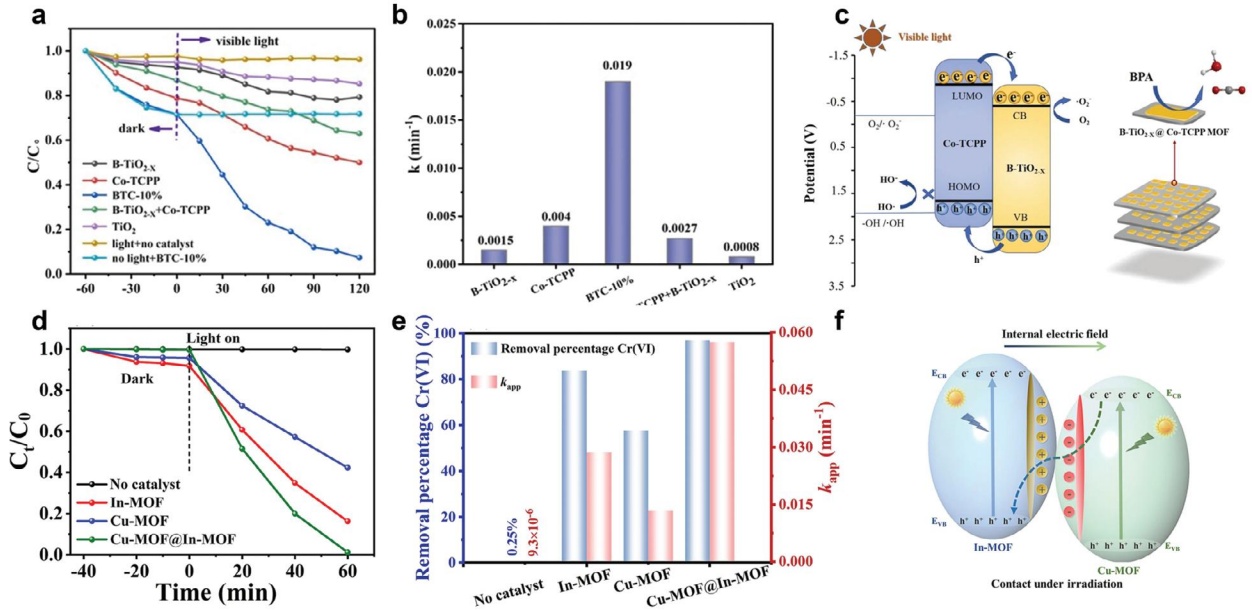

Figure 9. a) Photocatalytic activity and b) pseudo-first-order rate constant for BPA by TiO_2, B-TiO_{2-X}, Co-TCPP MOF, BTC-10%, and B-TiO_{2-X}+ Co-TCPP MOF. c) The possible photocatalytic degradation mechanism of BPA by BTC-10% composite under visible light irradiation. Reproduced with permission from ref.[67] Copyright 2021, Elsevier. d) Photocatalytic activities and e) removal percentage of the control group, In-MOF, Cu-MOF, and Cu-MOF@In-MOF catalysts under visible light irradiation. f) Schematic diagrams of charge transfer processes in Cu-MOF@In-MOF Z-scheme heterojunction under visible light irradiation. Reproduced with permission from ref.[70] Copyright 2023, Elsevier.

heterojunctions, which are crucial for the effective separation of electrons and holes. This process helps to reduce charge recombination, resulting in a significant improvement in photocatalytic degradation efficiency. For instance, the 2D-2D Co-TCPP MOF@B-TiO_2-X heterostructure with inherent electric field and bolstered visible light absorption demonstrated exceptional photocatalytic efficacy in degrading (BPA), achieving a degradation rate of up to 97% within 120 min of irradiation (**Figure 9**a).[67] This heterostructure showed degradation efficiencies 7.3 and 19.3 times higher than those of the individual Co-TCPP MOF and B-TiO_2−X components, respectively, with $\cdot O_2^-$ as the main active species (Figure 9b and c). The face-to-face arrangement in a 2D/2D heterostructure photocatalyst facilitates close and extensive contact between the two materials, promoting the separation and movement of photoinduced charges at the interface of the nanosheets. Additionally, the robust electronic coupling between the layers of the nanosheet further enhances photocatalytic performance. Consequently, effective charge transfer and adequate redox capability can be achieved in such 2D/2D heterostructure photocatalysts, like 2D/2D MOF-5/layered triple hydroxide (LTH) hybrid[68] and Ni-MOF/BiOCl heterojunctions,[69] which showed superior performance for the degradation of MB and TC with remarkable removal rate. These innovative heterostructures not only broaden the spectral response into the visible range but also enhance charge transport pathways, setting the stage for the development of highly efficient and durable 2D MOF-based photocatalytic systems.

In addition to photocatalytic degradation for organic pollution, 2D MOFs have also been applied as photocatalysts for the reduction of Cr(VI) to Cr(III) from contaminated environments. For instance, Tian et al.[70] introduced a "dimensionality-hybrid" 2D/3D Cu-MOF@In-MOF heterostructure with high specific surface area (718.1 $m^2\ g^{-1}$) and enhanced photo-absorption characteristics within the visible-light spectrum. The resulting Cu-MOF@In-MOF heterojunction demonstrated superior photocarrier separation and electron transfer efficiency, achieving a remarkable 98% photocatalytic reduction of Cr(VI) under visible-light irradiation, surpassing the performance of individual MOFs and many reported photocatalysts (Figure 9d–f). Moreover, the pH value significantly impacts the reduction of Cr(VI), with acidic solutions favoring the reduction of $HCrO_4^-$ or $Cr_2O_7^{2-}$ to Cr(III), while neutral and alkaline media promote the formation of CrO_4^{2-}, leading to the formation of $Cr(OH)_3$ on the catalyst surface, thereby hindering the reduction process.

Improved electron–hole separation and charge conversion can greatly enhance photocatalytic efficiency when the thickness of MOF materials is minimized to the atomic scale. This advantage arises from their effective mass transfer pathways, strong electron conduction capabilities, and plentiful active sites. In particular, 2D MOF nanosheets with ultrathin configuration provide an excellent platform for exploring the complexities of photocatalytic mechanisms. By fine-tuning variables such as thickness, lateral dimensions, functional groups, defects, and stability of 2D MOFs, one can delve into pioneering heterojunction designs based on advanced 2D MOFs, which can then be optimized for practical applications in photocatalysis.

4.3. Membrane-Based Separation

Nanosheets of 2D molecular sieves, commonly referred to as molecular sieve nanosheets, are regarded as highly promising

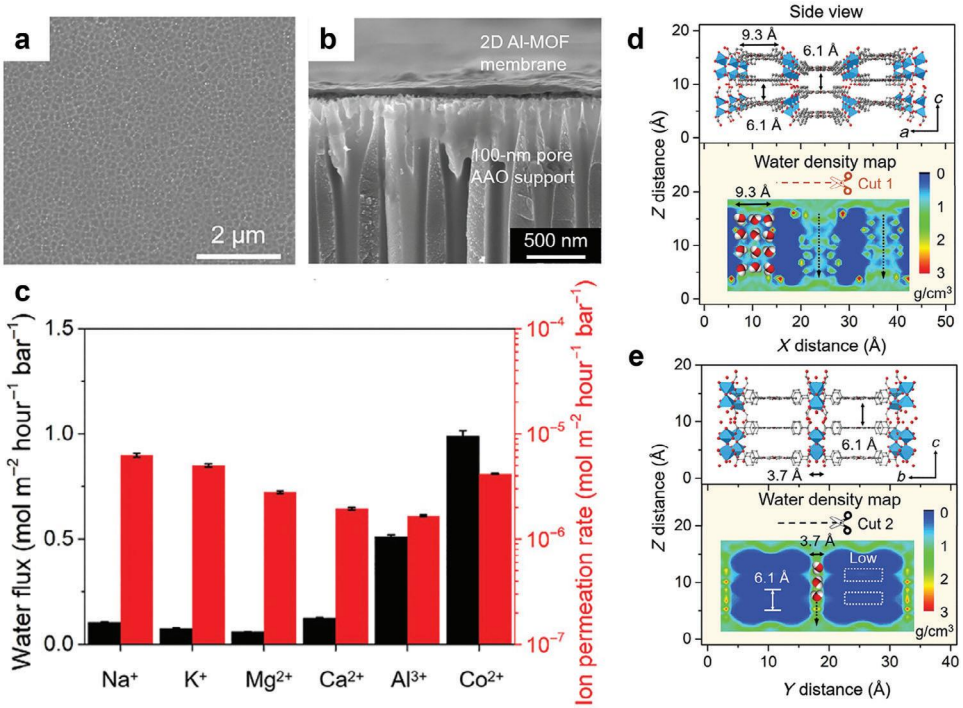

Figure 10. a) SEM image of Al-MOF laminar membrane. b) Cross-sectional image of Al-MOF laminar membrane on AAO substrate. Water flux and corresponding ion permeation rates of Al-MOF membrane using different draw solutions (0.5 M). Side view and corresponding water density map of the Al-MOF membrane along d) the [001] direction and e) [100] direction. [100] direction. Reproduced with permission from ref.[77] Copyright 2023, Science.

candidates for the development of membranes that exhibit remarkable selectivity and permeability. These membranes facilitate the passage of molecules with diverse sizes and shapes through the inherent pores present in the nanosheet plane and the interlayer galleries created by the stacking of nanosheets. Various types of molecular sieve nanosheets, such as graphene oxide (GO) and its derivatives, zeolites, MOFs, and covalent organic frameworks (COFs), have been utilized as key building blocks for ultrathin molecular sieve membranes.[71] MOF nanosheets are characterized by a composition of metal ions and organic ligands arranged within the sheet plane, offering a wide range of crystal structures and chemical functionalities. They feature a large specific surface area, an exceptionally thin profile of ≈1 nm for a monolayer), and well-sized pore arrays with high density. Additionally, they exhibit diverse pores, spanning nanopores to mesopores, allowing for customizable chemical properties in both in and out-of-plane orientations, among other advantages.[10a] Consequently, MOF nanosheets are increasingly considered more advantageous than other 2D molecular sieve materials for membrane fabrication.

MOF-based membranes can be categorized into three types: polycrystalline MOF membranes, MOF-based mixed matrix membranes, and MOF nanosheet membranes. Polycrystalline MOF membranes are primarily formed through the continuous growth (or deposition) of MOFs on a porous substrate. Theoretically, these membranes exhibit significant selectivity.[72] However, the uncontrolled growth of polycrystalline MOFs and incomplete coverage of the substrate often lead to the formation of intercrystalline defects or cracks within the membranes, adversely affecting their selectivity.[73] MOF-based mixed matrix membranes are created by blending dispersed MOFs with a continuous polymer matrix.[74] Nonetheless, due to the generally low porosity of most polymer matrices, the permeability of these membranes tends to be relatively low.[75] Additionally, phase segregation of MOFs within the polymer matrix is common, and the aggregation of MOF particles can result in the formation of void defects in the membrane.[76] MOF nanosheet membranes are assembled through the ordered stacking of 2D MOF nanosheets, driven by interlayer interactions. The exceptional physicochemical properties of these 2D MOF nanosheets render them ideal materials for constructing large-area, ultrathin MOF separation membranes. The vacuum filtration technique is frequently employed in the fabrication of 2D nanosheet membranes. In this process, a porous substrate is placed within a filtration apparatus, allowing the solvent from the nanoparticle suspension to pass through gently. Consequently, the 2D MOFs are deposited onto the substrate. In 2020, Jian et al.[77] pioneered the fabrication of ultrathin water-stable Al-MOF membranes using exfoliated 2D monolayer aluminum tetra-(4-carboxyphenyl) porphyrin framework (Al-MOF) nanosheets (**Figure 10**a,b). The nanopores of Al-MOF effectively block examined inorganic ions while allowing water molecules to penetrate based on size exclusion, resulting in a water flux of 2.2 mol m^{-2} h^{-1} bar^{-1} and rejection rates approaching 100% for investigated ions (Figure 10c). In another example, laminated 2D Cu-TCPP membranes with a thickness of 300 nm demonstrated a water permeance of 840.1 L·m^{-2}·h^{-1}·bar^{-1}, achieved a rejection rate of 99.9% for CR, and exhibited an exceptionally low rejection rate of less than 0.4% for salts.[78] Addition-

ally, the obtained membrane demonstrated high rejection rates exceeding 90% for small molecular dyes, including CV and CB-T. The morphologies, structures, and thicknesses of the lamellar membranes could be regulated by altering the lateral dimensions and loading amounts of the 2D MOF nanosheets, enabling the optimization of both membrane separation performance and antifouling characteristics.

In traditional separation membranes composed of 2D materials, the interlayer spacing between adjacent nanosheets plays a critical role in regulating both water transport and solute sieving capabilities. A meticulous balance in this interlayer spacing is essential, as it determines the magnitude of resistance that affects the diffusion of molecules through the membrane. Tighter spacings may hinder the flow of water and solutes, while excessively large spaces could compromise the selectivity of the separation process. In stark contrast, membranes constructed from 2D MOFs leverage the unique architectural features of the nanosheets, wherein the intrinsic nanopores embedded within the MOF structure serve as the primary determinants for ion and water separation. The vertically aligned aperture channels within the MOF nanosheets function as the principal conduits for water molecule transport, guiding the flow efficiently while maintaining a high degree of selectivity. For example, simulation results confirm that water flow is concentrated within the intrinsic pores of Al-MOF nanosheets in Al-MOF membranes. In this confined environment, water molecules align side by side, primarily moving through the vertically aligned aperture channels, with only a minimal shift flow of 17.08% occurring through the interlayer space (Figure 10d,e).[77] The NUS-8 membranes, oriented preferentially along the [001] direction, position the pore channels of the NUS-8 framework perpendicularly to the surface. This vertical alignment enables the effective uptake and transfer of molecules.[79] The separation and movement of water molecules within the NUS-8 membrane primarily occur through the vertical 1D pore channels of the NUS-8 framework, facilitated by the orderly arrangement of the nanosheets and their interlayer channels. Due to the presence of incomplete coordination of —COOH groups, the 2D MOF membrane surface displays negative charges across various aqueous pH levels, making it preferable to exclude negatively charged organic dyes.[80] Overall, the rejection can be explained by a synergistic effect that combines the molecular sieve properties with electrostatic rejection mechanisms.

In the realm of water treatment utilizing 2D MOF membranes, ensuring the membrane's stability and anti-fouling ability is of paramount importance to maintain efficiency and longevity. The stability of these membranes is intricately linked to the inherent stability of the MOFs utilized in their construction. Hence, it becomes imperative to meticulously choose MOF building units known for their superior water stability when fabricating 2D MOF membranes. Additionally, delving deeper into the interactions between the individual layers of 2D MOF structures emerges as a critical factor in bolstering the overall stability of the membranes. By fine-tuning these interactions, it is possible to substantially improve the durability and efficiency of 2D MOF membranes in water treatment applications. For instance, the 2D Cu-TCPP membrane reported by Cheng et al.[78] displayed exceptional chemical and physical stability, along with remarkable antifouling attributes during cross-flow filtration. The interaction among adjacent nanosheets in the membrane inhibited swelling, primarily due to the coordination of Cu^{2+} ions with carboxyl groups at nanosheet edges and defect sites, electrostatic attraction between Cu^{2+} or imino groups of the porphyrin ring, and carboxyl groups of the nanosheets, as well as van der Waals forces between neighboring nanosheets. The interaction of Cu^{2+} with water molecules enhances the creation of a layer of hydrated ions, leading to outstanding anti-fouling properties. Incorporating polymers or other nanomaterials is anticipated to further improve the stability of 2D MOF membranes. For example, polyvinyl alcohol (PVA) served as both a crosslinking agent and a spacer between the layers. Additionally, PVA significantly improved the bonding strength between the 2D Zn (BDC) nanosheets and the substrate.[80] By varying the concentration of PVA, it is possible to effectively regulate the membrane thickness, and layer spacing, thereby optimizing the selective separation performance of the laminated 2D Zn(BDC) membranes for dye molecules.

2D MOFs can also be applied as an intermediate layer in traditional polyamide nanofiltration membranes, significantly enhancing their performance. The nanosheets of 2D MOFs typically feature a significant number of hydrophilic groups, including carboxyl groups, coordinated water molecules, and bridging hydroxyl groups. Furthermore, the introduction of 2D MOF nanosheets enhances membrane roughness and modifies the membrane surface morphology from a nodular to a leaf-like structure.[81] As a result, the addition of hydrophilic 2D MOF nanosheets serves as an effective approach to modify the hydrophilicity and fouling resistance of the developed reverse osmosis membrane. The integration of 2D MOF nanosheets, which feature porous windows and interlamellar channels, greatly promotes the formation of numerous water pathways, thereby further improving the water permeability of the thin-film nanocomposite membrane. For example, a thin-film nanocomposite (TFN) membrane incorporating 0.015 wt% of nickel-based 2D MOF nanosheets in the selective layer demonstrates a water permeability that is 2.5 times greater than that of a pristine thin-film composite (TFC) membrane, while maintaining a comparable salt rejection rate.[81]

2D MOFs nanosheet membranes have garnered significant attention for their potential to achieve unprecedented levels of selectivity and permeability in separation processes, surpassing conventional polymer membranes. Integrating additional functionalities, such as photocatalysis and antibacterial properties, into these membranes holds promise for the development of multifunctional membranes, enhancing their applicability in various separation scenarios.[82] Despite notable advancements, optimizing membrane preparation strategies to regulate layer spacing, nanosheet stacking, and orientation, alongside minimizing film thickness, remains pivotal to fully harnessing the advantages of MOF nanosheets for practical separation applications.

4.4. Environmental Sensing

The luminescent characteristics of MOF materials, particularly those doped with rare earth elements, are significantly influenced by their framework structures, ion coordination environments, and the surface properties of the MOF channels. Additionally,

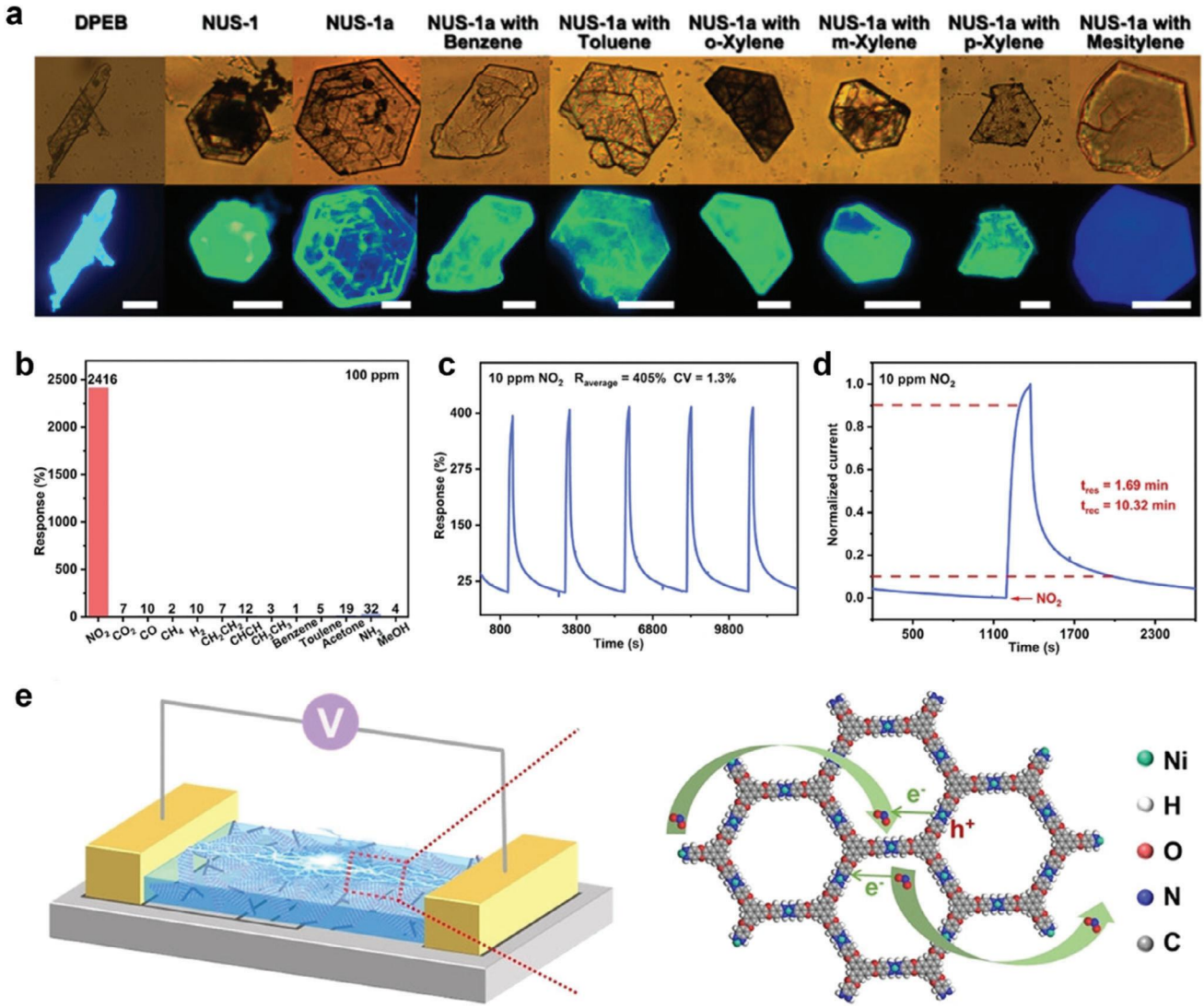

Figure 11. a) Optical images (top) and fluorescent images (bottom) of NUS-1a with different VOCs (scale bar, 30 μm). Reproduced with permission from ref.[84] Copyright 2014, American Chemical Society. b) Response-ability of HIOTP-Ni toward different gases. c) Response-recycle of HIOTP-Ni toward 10 ppm NO_2. d) Normalized response-recovery time curves of HIOTP-Ni for 10 ppm NO_2. e) The possible sensing mechanism of HIOTP-Ni for NO_2. Reproduced with permission from ref.[85] Copyright 2023, Wiley-VCH GmbH & Co.

these materials are highly sensitive to weak interactions between the framework and guest molecules, including hydrogen bonds, van der Waals forces, and π–π interactions. This sensitivity opens up their potential applications in fluorescence detection.[83] The elevated surface area of 2D nanosheets leads to a greater number of exposed active sites compared to bulk MOFs, which predominantly have active sites located within their pores and channels. This increased exposure enhances the interaction between substrate species and active sites. As a result, 2D MOFs have found extensive application in optical sensors, demonstrating exceptional performance.

The application of derived from 2D MOFs has progressively extended beyond the detection of small molecules and ions to include biological molecules, as well as temperature and pH sensing. This review focuses solely on environmentally relevant sensing applications. As early as 2014, turn-on responsive fluorescence characteristic was introduced into 2D MOFs (named NUS-1) with a tetraphenylethene-based ligand by Zhao and coworkers.[84] Significant shifts in the emission maxima were observed when NUS-1 crystals were exposed to UV light while immersed in solutions containing various volatile organic compounds (VOCs). This demonstrated the potential of these 2D MOFs to serve as effective fluorescent molecular sensors for the detection of VOCs (**Figure 11**a). Later in 2016, the luminescent 2D MOF nanosheets NTU-9-NS obtained via top–down method for the highly sensitive sensing of Fe^{3+} was reported by Xu et al. in 2016.[86] Notably, the response time was rapid, occurring within seconds, and these nanosheets demonstrated an impressive detection limit of 0.45 μM, outperforming other reported MOF materials. Additionally, the fluorescent 2D MOFs functioned as capable sensory materials, facilitating turn-off detection of explosive nitroaromatic compounds (NACs). In 2018, a photochromic 2D

layered In-TPA MOF nanosheet was reported by Moorthy and co-workers.[87] The 2D MOFs exhibited a notable fluorescence quantum yield of 0.15, while the fluorescence of their exfoliated nanosheets showed a quenching efficiency of 80%, allowing for the detection of electron-deficient trinitrotoluene (TNT) at ≈11 ppm. The various weak interactions between 2D MOF materials and guest molecules facilitate effective proximity between the two. Similar to many fluorescence sensors, the applications for fluorescence detection typically rely on mechanisms of fluorescence enhancement or quenching.[10b] Fluorescence quenching is largely dependent on electron transfer from excited MOFs to sulfonamides. For instance, when the lowest unoccupied molecular orbitals (LUMOs) are positioned between the valence band (VB) and the conduction band (CB) of the electron-rich InTP MOF, it becomes progressively easier to induce quenching of the electron-deficient analyte.[87] In this case, the photoexcitation results in the transfer of electrons from the CB of the TPA MOF to the LUMO of the electron-deficient analyte manifested as a decrease in fluorescence intensity due to an increase in the non-radiative decay rate. Therefore, In- TPA MOFs have a higher quenching rate for electron-deficient nitro-aromatic compounds.

The detection mechanism of chemical resistance sensors relies on transforming surface reactions into electrical signals, specifically resistance and conductance. 2D conjugated MOFs are employed in chemical resistance sensing because of their remarkable characteristics, which facilitate enhanced surface reactions and the adsorption of gas molecules.[88] In comparison to carbon-based nanomaterials, hybrid materials, and semiconductor metal oxides, chemoresistance sensors based on 2D conjugated MOFs exhibit high selectivity and can function effectively at room temperature. For example, the HIOTP-Ni MOF with a large pore aperture (3.3 nm) and high surface area (1300 $m^2 g^{-1}$) was reported by Chen et al.[85] This 2D MOF demonstrated outstanding capabilities as a chemiresistive sensor, exhibiting a remarkable selectivity of 405% and a swift response time of 1.69 min when detecting 10 ppm of NO_2 at room temperature (Figure 11b–d). Additionally, Smith and Mirica developed multifunctional electronic textiles for the detection of gases by incorporating a conductive 2D MOF on textiles (SOFT).[89] The resulting SOFT device demonstrated the ability to effectively detect and differentiate between NO and H_2S at parts per million (ppm) levels, with limits of detection (LOD) of 0.16 ppm for NO and 0.23 ppm for H_2S. Additionally, they introduced a series of reticular bimetallic conductive 2D MOFs derived from nickel phthalocyanine and nickel naphthalocyanine, which serve as active components for the detection of gases such as NH_3, H_2S, and NO.[90] These devices exhibited remarkable sensitivity, achieving detection limits ranging from sub-part-per-million (ppm) to parts per billion (ppb) for NH_3 (0.31–0.33 ppm), H_2S (19–32 ppb), and NO (1.0–1.1 ppb). The chemical sensing mechanism of 2D MOFs for gaseous analytes is a sophisticated process that primarily involves intricate surface interactions between the analytes and the material's surface, as well as underlying electronic phenomena such as charge transfer and redox reactions. When gaseous molecules encounter the surface of 2D MOFs, specific adsorption occurs, leading to alterations in the local electronic structure and surface potentials. This interaction not only affects the adsorption energy but also modulates the electronic pathways available for charge transfer. Consequently, the interaction may cause a shift in the population of charge carriers within the MOF, resulting in significant changes in its electrical conductivity. In many cases, the extent of these conductivity alterations serves as an indicator of the concentration and nature of the analyte, making 2D MOFs highly sensitive to even minute fluctuations in gaseous environments. For instance, the chemiresistive sensor utilizing HIOTP-Ni can rapidly adsorb NO_2 and transfer electrons, leading to an increased concentration of holes within the HIOTP-Ni, which subsequently changes its electrical conductivity. Consequently, when NO_2 was removed from the HIOTP-Ni, the captured electrons could return to the framework, aiding in the recovery of the current (Figure 11e).[85] The capacity to modify its structure by altering precursors offers a variety of properties that are suitable for numerous applications. Furthermore, electrochemically active 2D MOFs can be synthesized by integrating redox-active metal nodes or organic ligands. For example, the exposure of NiPc-M MOFs to H_2S led to a reduction in the organic ligands, as shown by a decrease in C═O bonds and changes in EPR signal intensity, while exposure to NO resulted in the oxidation of metal centers in NiPc-Cu and the ligand in NiPc-Ni, highlighting the dynamic response of the MOFs to different gas environments.[90] In addition, the possible open coordination on the metal center can be used as the active site for the analyte binding.[91] The hydrated ligands at the metal center may also establish hydrogen bonds with the analyte.[92] Defects at the edges of 2D MOFs and the presence of overhanging coordination sites also have an impact.

4.5. Disinfection

MOF-based materials are currently a focal point in the realm of disinfection. In contrast to conventional antibacterial agents, they offer several advantages: first, MOFs can be synthesized using bactericidal metal ions like Ag^+, Zn^{2+}, Co^{2+}, and Cu^{2+}, along with certain organic substances such as imidazoles (IMIs) and porphyrins, allowing for sustained and controlled release based on environmental cues, like pH reduction and laser exposure.[93] Second, the versatility of incorporating diverse metal and organic constituents into the structure of photocatalytic MOFs leads to the creation of a range of HOMO–LUMO energy gaps conducive to generating different types of ROS, thereby enhancing antimicrobial efficacy through photocatalysis.[94] Furthermore, the chelation properties of MOFs lower the metal ions' polarity, increasing their lipophilicity and enabling them to effectively penetrate bacterial membranes to kill pathogens. Additionally, the nanoscale MOFs exhibit low toxicity, biodegradability, and excellent dispersibility, expanding their potential applications in disinfection.

2D MOF-based antibacterial materials not only possess the structural benefits of MOF materials seamlessly. When compared to 3D MOF particles, 2D MOF nanosheets demonstrate a higher abundance of active sites, an effective light-harvesting framework, and rapid energy transfer, due to their relatively larger surface area. As a result, these materials exhibit improved antibacterial properties. For instance, the presence of surface copper sites encourages attachment and interaction with pathogens, enhancing physical contact with the microorganisms. Quasi-2D Cu-BTC MOFs demonstrated remarkable antimicrobial effective-

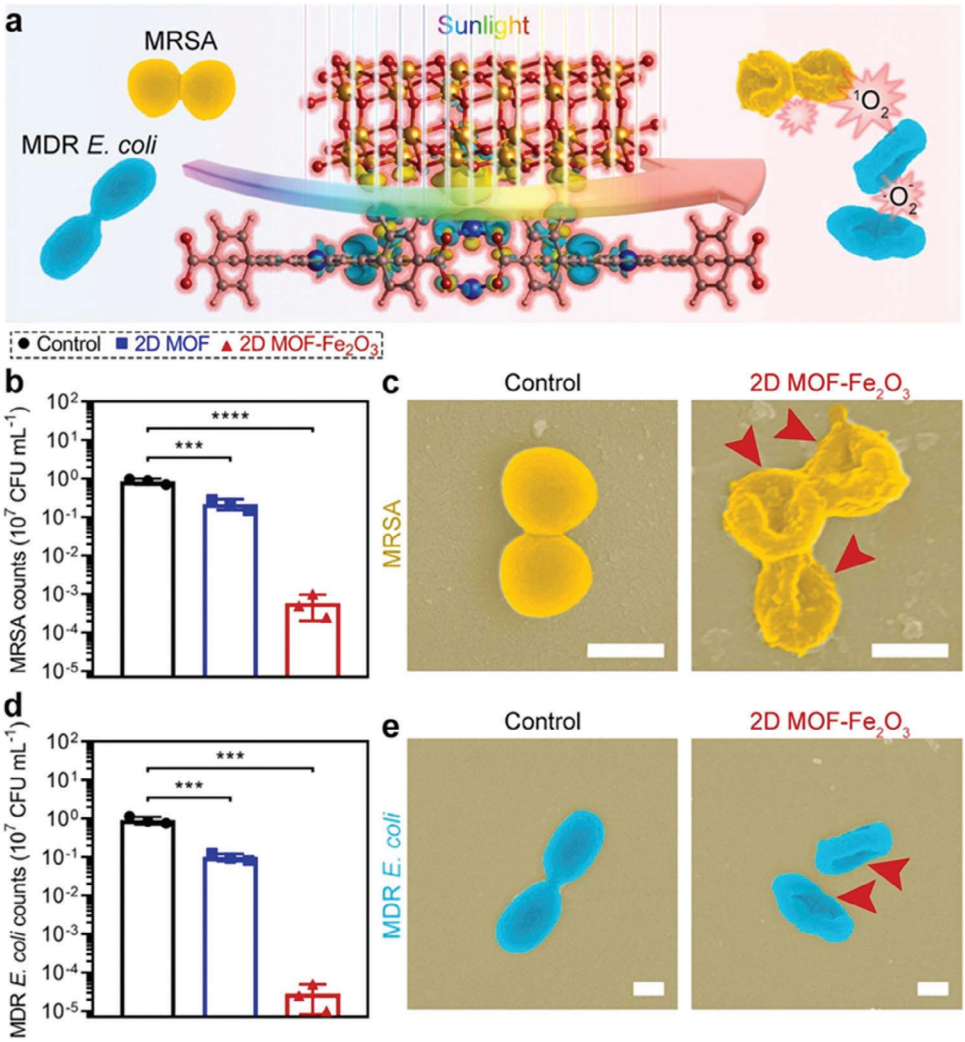

Figure 12. a) Schematic diagram illustrating the photocatalytic antibacterial mechanism of 2D MOF-Fe_2O_3. Viabilities of b) MRSA and d) MDR *E. coli* treated with 2D MOF and 2D MOF-Fe_2O_3 under solar light irradiation for 20 min, respectively. c) SEM images of MRSA and e) MDR *E. coli* treated with 2D MOF-Fe_2O_3 under solar light irradiation for 20 min (scale bars = 500 nm). Reproduced with permission from ref.[95] Copyright 2022, Elsevier.

ness against three chosen plant pathogens, achieving minimal inhibitory concentrations (MICs) that are half those of a commercial pesticide and one-eighth that of their conventional 3D cubic MOF counterparts.[96] Furthermore, establishing antibacterial surfaces based on 2D MOFs can prevent or eradicate bacteria before they adhere to the membrane surface, effectively mitigating membrane biological contamination.[97]

An elevated degree of porosity and a distinct specific surface area can significantly improve the effective encapsulation and loading of various substances within their pores. Moreover, an abundance of surface active groups can aid in modifying other materials on their surface, which is advantageous for creating MOFs-based dual-effect antimicrobial composites. The intricate and diverse antibacterial mechanisms of MOFs enable the design of a single MOF material with combined antimicrobial effects, such as physical and chelation, photocatalytic activities, and metal ion release.[93] The creation of heterointerfaces based on 2D photonic MOFs via surface engineering may offer a promising strategy to improve their antimicrobial efficacy. For instance, the heterostructure of 2D ZnTCPPMOF-Fe_2O_3 significantly adjusted the band structure and density of states of 2D ZnTCPP MOF.[95] Under solar light irradiation, the heterointerface facilitated the transfer of multiple photoelectrons from the 2D ZnTCPP MOF to Fe_2O_3, functioning with the 2D ZnTCPP MOF as the electron donor and Fe_2O_3 serving as the acceptor (**Figure 12**a). This improved charge transfer mechanism can prolong the duration of photogenerated charges, consequently boosting the photocatalytic disinfection efficiency, achieving antibacterial effectiveness greater than 99.9% within 20 min against MRSA and multidrug-resistant *E. coli* (Figure 12b–e). In another case, A heterojunction of Fe_2O_3-modified porphyrinic MOFs (CuTCPP-Fe_2O_3) formed via atomic-layer deposition demonstrated extensive antimicrobial activity, achieving 99.87±0.09%, 99.57±0.21%, and 99.03 ± 0.24% effectiveness against a range of pathogens, including *Porphyromonas gingivalis*, *Fusobacterium nucleatum*, and *Staphylococcus aureus*. The remarkable antibacterial effect could be attributed to the synergistic interactions between ROS and the released metal ions. Initially, exposure to

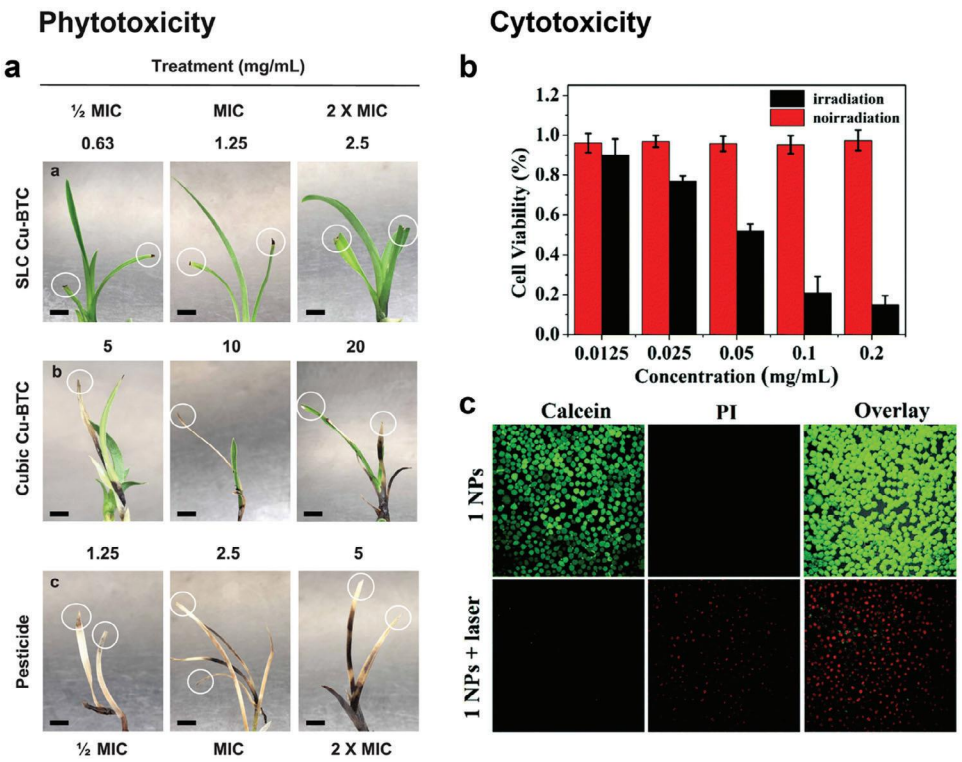

Figure 13. a) Effect of SLC Cu-BTC, cubic Cu-BTC MOFs, and the commercial pesticide on the expression of *Odontoglossum* ringspot virus (ORSV) and symptoms of orchid *Cymbidium*. Reproduced with permission from ref.[96] Copyright 2021, American Chemical Society. b) Quantitative detection of cell viability with MOF nanosheets. c) Fluorescence images of calcein AM/PI co-stained MCF-7 cells treated with MOF nanosheets with/without light irradiation. Reproduced with permission from ref.[99] Copyright 2020, Royal Society of Chemistry.

light rapidly generated singlet oxygen ($^1O_2$), which subsequently compromised the structural integrity of the bacterial membrane, resulting in increased permeability. Furthermore, the released metal ions, including Cu^{2+} and Fe^{3+}, were capable of swiftly infiltrating the compromised bacterial membrane and entering the bacterial cells, thereby disrupting their metabolic processes.[98]

5. Environmental Implications

As research advances in the field of 2D MOF-based nanomaterials and devices, it becomes essential to examine the behavior of 2D MOF nanosheets upon their release into the environment. Nanomaterials can experience considerable chemical and physical transformations, including dissolution, oxidation, aggregation, sulfidation, and deposition, influenced by their specific chemical phase, composition, and surface characteristics within natural biological and environmental contexts. The dissolution of nanomaterials is particularly noteworthy, as it can produce soluble compounds that are readily available and potentially detrimental to both aquatic life and human health. Furthermore, if these nanomaterials are persistent and resistant to biodegradation, they could represent a long-term environmental threat. MOFs containing nodes with antimicrobial metal ions like Ag^+, Co^{2+}, Cu^{2+}, and Zn^{2+} have been utilized as antimicrobial agents due to their decreased toxicity relative to freely dissolved metal ions. For example, Cu-BTC MOF not only exhibited potent broad-spectrum antimicrobial properties, especially against plant pathogens, but also demonstrated minimal harm to plants when used preventively or therapeutically against fungal, bacterial, and viral infections.[96] Extensive monitoring over months revealed no adverse effects (e.g., discoloration, spotting, tissue death) from the use of SLC Cu-BTC MOF on overall plant well-being at any point (**Figure 13a**). Through sonication exfoliation, 2D Ca-TCPP nanosheets can efficiently infiltrate cells, demonstrating excellent biocompatibility.[99] The viability of MCF-7 cells remained stable (≈95%) throughout the experiment without exposure to white light, indicating that Ca-TCPP nanosheets did not exhibit cell toxicity as concentrations increased (Figure 13b,c). The potential toxicity of MOFs warrants thorough consideration, necessitating a comprehensive evaluation to advance practical applications. While certain MOF-based substances have been safely administered to mice in short-term in vivo trials, sustained toxicity must be addressed for specific practical uses. Mitigating MOF toxicity by opting for naturally occurring metal ions and biocompatible organic linkers could prove to be an effective approach.

6. Conclusion and Future Perspectives

The increasing enthusiasm for employing 2D MOF nanomaterials in environmental applications has arisen from the impressive discoveries regarding the unique properties and efficacy of bulk MOFs and nanomaterials derived from graphene. As previously mentioned, the distinct properties of 2D MOF nanosheets are anticipated to offer various environmental advantages that cannot

be achieved through the use of bulk MOFs and graphene-derived nanomaterials. Although still in the early stages, investigations into the utilization of 2D MOF nanomaterials have already shown potential applications such as pollutant adsorption, contaminant photodegradation, membrane separation, sensing, and disinfection. To optimize the benefits and mitigate the drawbacks of 2D MOF nanomaterials in environmental use, numerous key research queries related to their unique adsorption, photodegradation, semiconductor, and filtration capabilities need resolution, and the accompanying mechanisms must be comprehensively grasped.

In the realm of adsorption, 2D MOFs encounter challenges akin to those faced by traditional adsorbents, namely fouling in practical settings and the recovery of nanoscale adsorbents from water for reuse. In an ideal scenario, the chemically exfoliated 2D MOF monolayer emerges as an exceptionally promising adsorbent for pollutants. However, extracting the 2D MOF monolayer from water poses a significant challenge. Possible methods for recovering the adsorbent include attaching magnetic nanoparticles, bonding nanosheets to the surfaces of other porous materials, and designing a 3D macroscopic structure that incorporates these nanosheets as fundamental building blocks. Furthermore, the different synthesis techniques provide 2D MOFs with a range of complex surface chemistries (such as negative charge, phase variations, specific functional groups, and defects), and the effects of these characteristics on contaminant adsorption efficiency require thorough investigation. This research is essential for guiding the systematic advancement of high-performance 2D MOF-based adsorbents. The application of 2D MOFs for the removal of environmentally significant substances, extending beyond heavy metals and organic pollutants, as discussed in this review, is still largely uncharted territory. Various environmental factors, including ionic strength, pH levels, and natural organic matter (NOM), can affect both the adsorption capacity and kinetics of 2D MOF adsorbents, warranting further exploration in future research.

While a few initial findings have indicated the potential for photocatalytic remediation or sterilization with 2D MOFs and similar materials, thorough exploration is still needed. Particularly, ultrathin 2D MOF nanosheets present a sturdy foundation for scrutinizing the complexities of photocatalytic mechanisms. Through meticulous adjustments of parameters like thinness, lateral measurements, functional moieties, imperfections, and durability of 2D MOFs, researchers can pioneer innovative heterojunction configurations using cutting-edge 2D MOFs that are poised for optimization in real-world applications involving photocatalysis. Additional investigations are warranted to enhance comprehension of the bandgap architectures of 2D MOFs produced through diverse methods, varieties of catalytically induced ROS, the byproducts of 2D MOFs-mediated decontamination with and without full breakdown, and the resistance of 2D MOF nanosheets to light-induced degradation. Consequently, there is a clear call for further exploration in the realm of 2D MOF photocatalytic uses.

The utilization of 2D MOFs for membrane applications is still in its initial stages. An arrangement of 2D MOF-based membranes in layers showcases significant potential for achieving elevated water flow rates, precisely adjustable interlayer distances, robust structural integrity resistant to swelling or compression, and outstanding resistance to fouling from organic substances. Further investigation is essential to probe these intriguing properties and explore their connections with the distinct characteristics of 2D MOF nanosheets, which differ markedly from those of GO nanosheets. These disparities include the rigid nature of 2D MOFs versus the flexibility of GO, as well as the porous structure of 2D MOFs in contrast to the relatively dense composition of GO with protruding oxygenated functional groups. A thorough understanding of the interlayer spaces, the accessible areas within the 2D MOF membrane, the movement of molecules and ions through the 2D channels, the core principles that dictate separation, and the mechanisms that contribute to resistance against fouling is essential. This necessitates a systematic exploration through empirical analysis coupled with molecular dynamics simulations.

Consideration of both the production cost and environmental impact is crucial when advancing 2D MOF nanomaterials for environmental purposes. Currently, the cost associated with creating MOF nanosheets, particularly top-tier products crafted through the Solvothermal technique, surpasses that of numerous extensively researched materials in the environmental realm. However, it is anticipated that costs will decrease as synthesis methodologies are enhanced, production scales up, and the supply chain undergoes optimization. Enhancing the stability of 2D MOFs is vital. Comprehensive studies on the stability of 2D MOFs under various harsh conditions, including strong acids, basic electrolytes, and oxidative environments, are necessary to fully comprehend and improve their environmental resilience, thereby broadening their practical applications. To enhance the stability of 2D MOFs, it is essential to reinforce the interactions between metal nodes and organic ligands, particularly by employing high-valence metal ions (such as Zr^{4+}) that create robust Zr—O bonds and multiple chelating linkages. The post-synthetic modification process can also serve as a promising method to enhance the stability of 2D MOFs. However, related research remains limited. Additionally, it is crucial to conduct a comprehensive analysis of the environmental impacts, changes, and possible health hazards associated with 2D MOF nanosheets to reduce their ecological footprint. While initial findings suggest minimal toxicity associated with 2D MOFs, the diverse characteristics of these nanosheets—including thickness, lateral dimensions, phase variations, and defects—could complicate toxicity assessments, necessitating comprehensive future investigations to unravel the effects and their underlying mechanisms.

In conclusion, 2D MOF nanosheets represent an intriguing graphene-inspired inorganic material with distinct and innovative applications in various environmental domains, as elucidated by early research endeavors. As research progresses, the expanding exploration into 2D MOF nanomaterials is poised to yield compelling opportunities and advancements in environmental applications, contingent upon the dedicated pursuit of scientific objectives outlined in this review. In addition, several promising interdisciplinary research avenues present significant potential for advancing the application of 2D MOFs in environmental remediation. Notably, the integration of 2D MOFs with nanomaterials like graphene and carbon nanotubes can yield composite materials that enhance mechanical strength, surface area, and pore accessibility for superior pollutant removal. Furthermore, employing machine learning techniques for material

design enables efficient analysis of extensive datasets, facilitating the discovery and optimization of tailor-made 2D MOFs for specific environmental challenges. This multidisciplinary approach enhances material performance and offers innovative solutions to global water scarcity and pollution issues.

Acknowledgements

L.Lu. and L.Li. contributed equally to this work. Financial support from National Natural Science Foundatio of China (22106136, 22306172, 22376158, 42377489, 42007390), Basic and Applied Basic Research Foundation of Guangdong Province (2023A1515012650), Zhejiang Provincial Natural Science Foundation of China (LQ23E080007, LR24B070001), and Guangzhou Science and Technology Bureau (2023A04J0254) are highly appreciated.

Conflict of Interest

The authors declare no conflict of interest.

Keywords

2D, metal–organic frameworks, pollutant removal, porous structure, water purification

Received: October 14, 2024
Revised: October 31, 2024
Published online:

[1] a) X. Huang, M. Auffan, M. J. Eckelman, M. Elimelech, J.-H. Kim, J. Rose, K. Zuo, Q. Li, P. J. J. Alvarez, *Nat. Rev. Earth Environ.* **2024**, *5*, 572; b) D. L. Plata, N. Z. Janković, *Nat. Nanotechnol.* **2021**, *16*, 612; c) A. A. Keller, A. Ehrens, Y. Zheng, B. Nowack, *Nat. Nanotechnol.* **2023**, *18*, 834.
[2] a) L. Hu, W. Wu, M. Hu, L. Jiang, D. Lin, J. Wu, K. Yang, *Nat. Commun.* **2024**, *15*, 3204; b) L. Jiao, J. Y. R. Seow, W. S. Skinner, Z. U. Wang, H.-L. Jiang, *Mater. Today* **2019**, *27*, 43; c) H. A. Almassad, R. I. Abaza, L. Siwwan, B. Al-Maythalony, K. E. Cordova, *Nat. Commun.* **2022**, *13*, 4873.
[3] a) H. Hu, Z. Wang, L. Cao, L. Zeng, C. Zhang, W. Lin, C. Wang, *Nat. Chem.* **2021**, *13*, 358; b) Y. He, Z. Wang, H. Wang, Z. Wang, G. Zeng, P. Xu, D. Huang, M. Chen, B. Song, H. Qin, Y. Zhao, *Coord. Chem. Rev.* **2021**, *429*, 213618.
[4] O. M. Yaghi, H. Li, *J. Am. Chem. Soc.* **1995**, *117*, 10401.
[5] a) N. Stock, S. Biswas, *Chem. Rev.* **2012**, *112*, 933; b) S. Wang, C. M. McGuirk, A. d'Aquino, J. A. Mason, C. A. Mirkin, *Adv. Mater.* **2018**, *30*, 1800202.
[6] Z.-Q. Li, L.-G. Qiu, W. Wang, T. Xu, Y. Wu, X. Jiang, *Inorg. Chem. Commun.* **2008**, *11*, 1375.
[7] a) S. Song, W. Wang, Y. Zhao, W. Wu, Y. Wei, H. Wang, *Angew. Chem., Int. Ed.* **2023**, *135*, 202312995; b) K. Ge, S. Sun, Y. Zhao, K. Yang, S. Wang, Z. Zhang, J. Cao, Y. Yang, Y. Zhang, M. Pan, L. Zhu, *Angew. Chem., Int. Ed.* **2021**, *133*, 12204; c) J. E. Chen, Z.-J. Yang, H. U. Koh, J. Shen, Y. Cai, Y. Yamauchi, L.-H. Yeh, V. Tung, K. C.-W. Wu, *Adv. Mater. Interfaces* **2022**, *9*, 2102560.
[8] S. Zhao, Y. Wang, J. Dong, C.-T. He, H. Yin, P. An, K. Zhao, X. Zhang, C. Gao, L. Zhang, J. Lv, J. Wang, J. Zhang, A. M. Khattak, N. A. Khan, Z. Wei, J. Zhang, S. Liu, H. Zhao, Z. Tang, *Nat. Energy* **2016**, *1*, 16184.
[9] a) J. H. Kim, S. Wu, L. Zdrazil, N. Denisov, P. Schmuki, *Angew. Chem., Int. Ed.* **2024**, *136*, 202319255; b) Y.-z. Li, Z.-h. Fu, G. Xu, *Coord. Chem. Rev.* **2019**, *388*, 79; c) T. Rodenas, I. Luz, G. Prieto, B. Seoane, H. Miro, A. Corma, F. Kapteijn, F. X. Llabrés i Xamena, J. Gascon, *Nat. Mater.* **2015**, *14*, 48; d) H. Song, Y. Peng, C. Wang, L. Shu, C. Zhu, Y. Wang, H. He, W. Yang, *Angew. Chem., Int. Ed.* **2023**, *135*, 202218472.
[10] a) Y. Peng, W. Yang, *Adv. Mater. Interfaces* **2020**, *7*, 1901514; b) Y. Zheng, F.-Z. Sun, X. Han, J. Xu, X.-H. Bu, *Adv. Opt. Mater.* **2020**, *8*, 2000110; c) U. Khan, A. Nairan, J. Gao, Q. Zhang, *Small Struct.* **2023**, *4*, 2200109; d) L. Wang, S. E. Saji, L. Wu, Z. Wang, Z. Chen, Y. Du, X.-f. Yu, H. Zhao, Z. Yin, *Small* **2022**, *18*, 2201642.
[11] S. M. Moosavi, A. Nandy, K. M. Jablonka, D. Ongari, J. P. Janet, P. G. Boyd, Y. Lee, B. Smit, H. J. Kulik, *Nat. Commun.* **2020**, *11*, 4068.
[12] H. Furukawa, K. E. Cordova, M. O'Keeffe, O. M. Yaghi, *Science* **2013**, *341*, 1230444.
[13] Y. Peng, Y. Li, Y. Ban, W. Yang, *Angew. Chem., Int. Ed.* **2017**, *56*, 9757.
[14] M. Zhao, Y. Wang, Q. Ma, Y. Huang, X. Zhang, J. Ping, Z. Zhang, Q. Lu, Y. Yu, H. Xu, Y. Zhao, H. Zhang, *Adv. Mater.* **2015**, *27*, 7372.
[15] a) R. Sakamoto, K. Hoshiko, Q. Liu, T. Yagi, T. Nagayama, S. Kusaka, M. Tsuchiya, Y. Kitagawa, W.-Y. Wong, H. Nishihara, *Nat. Commun.* **2015**, *6*, 6713; b) T. Kambe, R. Sakamoto, K. Hoshiko, K. Takada, M. Miyachi, J.-H. Ryu, S. Sasaki, J. Kim, K. Nakazato, M. Takata, H. Nishihara, *J. Am. Chem. Soc.* **2013**, *135*, 2462.
[16] Y. Wang, L. Li, L. Yan, X. Gu, P. Dai, D. Liu, J. G. Bell, G. Zhao, X. Zhao, K. M. Thomas, *Chem. Mater.* **2018**, *30*, 3048.
[17] J.-C. Tan, P. J. Saines, E. G. Bithell, A. K. Cheetham, *ACS Nano* **2012**, *6*, 615.
[18] S. He, Y. Chen, Z. Zhang, B. Ni, W. He, X. Wang, *Chem. Sci.* **2016**, *7*, 7101.
[19] Q. Qi, J. Hu, Y. Zhang, W. Li, B. Huang, C. Zhang, *Adv. Energy Sustain. Res.* **2021**, *2*, 2000067.
[20] R. Makiura, S. Motoyama, Y. Umemura, H. Yamanaka, O. Sakata, H. Kitagawa, *Nat. Mater.* **2010**, *9*, 565.
[21] L. Zhang, G. Ng, N. Kapoor-Kaushik, X. Shi, N. Corrigan, R. Webster, K. Jung, C. Boyer, *Angew. Chem., Int. Ed.* **2021**, *60*, 22664.
[22] W. Wu, L. Wang, Y. Li, F. Zhang, L. Lin, S. Niu, D. Chenet, X. Zhang, Y. Hao, T. F. Heinz, J. Hone, Z. L. Wang, *Nature* **2014**, *514*, 470.
[23] Y. Peng, Y. Li, Y. Ban, H. Jin, W. Jiao, X. Liu, W. Yang, *Science* **2014**, *346*, 1356.
[24] P. Priyadarshini, K. Parida, *J. Energy Storage* **2024**, *87*, 111379.
[25] a) Y. Wang, M. Zhao, J. Ping, B. Chen, X. Cao, Y. Huang, C. Tan, Q. Ma, S. Wu, Y. Yu, Q. Lu, J. Chen, W. Zhao, Y. Ying, H. Zhang, *Adv. Mater.* **2016**, *28*, 4149; b) L. Cao, Z. Lin, F. Peng, W. Wang, R. Huang, C. Wang, J. Yan, J. Liang, Z. Zhang, T. Zhang, L. Long, J. Sun, W. Lin, *Angew. Chem., Int. Ed.* **2016**, *55*, 4962.
[26] H. Lin, Y. Yang, B. G. Diamond, T.-H. Yan, V. I. Bakhmutov, K. W. Festus, P. Cai, Z. Xiao, M. Leng, I. Afolabi, G. S. Day, L. Fang, C. H. Hendon, H.-C. Zhou, *J. Am. Chem. Soc.* **2024**, *146*, 1491.
[27] F. Ambroz, T. J. Macdonald, V. Martis, I. P. Parkin, *Small Methods* **2018**, *2*, 1800173.
[28] B. S. Yeo, A. T. Bell, *J. Am. Chem. Soc.* **2011**, *133*, 5587.
[29] J. Duan, S. Chen, C. Zhao, *Nat. Commun.* **2017**, *8*, 15341.
[30] Q. Hu, X. Huang, Z. Wang, G. Li, Z. Han, H. Yang, X. Ren, Q. Zhang, J. Liu, C. He, *J. Mater. Chem. A* **2020**, *8*, 2140.
[31] L. Xiao, Z. Wang, J. Guan, *Coord. Chem. Rev.* **2022**, *472*, 214777.
[32] M. Ding, X. Cai, H.-L. Jiang, *Chem. Sci.* **2019**, *10*, 10209.
[33] S. Yuan, J.-S. Qin, C. T. Lollar, H.-C. Zhou, *ACS Cent. Sci.* **2018**, *4*, 440.
[34] J. H. Cavka, S. Jakobsen, U. Olsbye, N. Guillou, C. Lamberti, S. Bordiga, K. P. Lillerud, *J. Am. Chem. Soc.* **2008**, *130*, 13850.
[35] Q. Ma, T. Zhang, B. Wang, *Matter* **2022**, *5*, 1070.
[36] X. Tian, F. Li, Z. Tang, S. Wang, K. Weng, D. Liu, S. Lu, W. Liu, Z. Fu, W. Li, H. Qiu, M. Tu, H. Zhang, J. Li, *Nat. Commun.* **2024**, *15*, 2920.
[37] J. Liu, Z. Wang, P. Cheng, M. J. Zaworotko, Y. Chen, Z. Zhang, *Nat. Rev. Chem.* **2022**, *6*, 339.
[38] H. Yuan, G. Liu, Z. Qiao, N. Li, P. J. S. Buenconsejo, S. Xi, A. Karmakar, M. Li, H. Cai, S. J. Pennycook, D. Zhao, *Adv. Mater.* **2021**, *33*, 2101257.

[39] H. Zhou, L. Zhang, G. Wang, Y. Zhang, X. Wang, M. Li, F. Fan, Y. Li, T. Wang, X. Zhang, Y. Fu, *ACS Appl. Mater. Interfaces* **2021**, *13*, 39755.
[40] a) C. Hermosa, B. R. Horrocks, J. I. Martínez, F. Liscio, J. Gómez-Herrero, F. Zamora, *Chem. Sci.* **2015**, *6*, 2553; b) X. Wang, C. Chi, K. Zhang, Y. Qian, K. M. Gupta, Z. Kang, J. Jiang, D. Zhao, *Nat. Commun.* **2017**, *8*, 14460.
[41] D. Liu, B. Liu, C. Wang, W. Jin, Q. Zha, G. Shi, D. Wang, X. Sang, C. Ni, *ACS Sustain. Chem. Eng.* **2020**, *8*, 2167.
[42] K. Jayaramulu, J. Masa, D. M. Morales, O. Tomanec, V. Ranc, M. Petr, P. Wilde, Y.-T. Chen, R. Zboril, W. Schuhmann, R. A. Fischer, *Adv. Sci.* **2018**, *5*, 1801029.
[43] Y. Ding, Y.-P. Chen, X. Zhang, L. Chen, Z. Dong, H.-L. Jiang, H. Xu, H.-C. Zhou, *J. Am. Chem. Soc.* **2017**, *139*, 9136.
[44] a) L. Majidi, A. Ahmadiparidari, N. Shan, S. N. Misal, K. Kumar, Z. Huang, S. Rastegar, Z. Hemmat, X. Zou, P. Zapol, J. Cabana, L. A. Curtiss, A. Salehi-Khojin, *Adv. Mater.* **2021**, *33*, 2004393; b) C. Tan, K. Yang, J. Dong, Y. Liu, Y. Liu, J. Jiang, Y. Cui, *J. Am. Chem. Soc.* **2019**, *141*, 17685; c) P. Chandrasekhar, A. Mukhopadhyay, G. Savitha, J. N. Moorthy, *J. Mater. Chem. A* **2017**, *5*, 5402; d) C. Wang, C. He, Y.-H. Luo, S. Su, J.-Y. Wang, D.-L. Hong, X.-T. He, C. Chen, B.-W. Sun, *Chem. Eng. J.* **2020**, *379*, 122337; e) L.-L. Liu, J. Chen, Y. Zhang, C.-X. Yu, W. Du, X.-Q. Sun, J.-L. Zhang, F.-L. Hu, Y. Mi, L.-F. Ma, *J. Mater. Chem. A* **2021**, *9*, 546; f) W. Zhang, Y. Wang, H. Zheng, R. Li, Y. Tang, B. Li, C. Zhu, L. You, M.-R. Gao, Z. Liu, S.-H. Yu, K. Zhou, *ACS Nano* **2020**, *14*, 1971. g) Y. Shen, B. Shan, H. Cai, Y. Qin, A. Agarwal, D. B. Trivedi, B. Chen, L. Liu, H. Zhuang, B. Mu, S. Tongay, *Adv. Mater.* **2018**, *30*, 1802497; h) J. Huang, Y. Li, R.-K. Huang, C.-T. He, L. Gong, Q. Hu, L. Wang, Y.-T. Xu, X.-Y. Tian, S.-Y. Liu, Z.-M. Ye, F. Wang, D.-D. Zhou, W.-X. Zhang, J.-P. Zhang, *Angew. Chem., Int. Ed.* **2018**, *57*, 4632; i) Y. Wen, Q. Liu, S. Su, Y. Yang, X. Li, Q.-L. Zhu, X. Wu, *Nanoscale* **2020**, *12*, 12767; j) R. Dong, M. Pfeffermann, H. Liang, Z. Zheng, X. Zhu, J. Zhang, X. Feng, *Angew. Chem., Int. Ed.* **2015**, *54*, 12058; k) L. Huang, X. Zhang, Y. Han, Q. Wang, Y. Fang, S. Dong, *J. Mater. Chem. A* **2017**, *5*, 18610; l) L. Zhao, B. Dong, S. Li, L. Zhou, L. Lai, Z. Wang, S. Zhao, M. Han, K. Gao, M. Lu, X. Xie, B. Chen, Z. Liu, X. Wang, H. Zhang, H. Li, J. Liu, H. Zhang, X. Huang, W. Huang, *ACS Nano* **2017**, *11*, 5800; m) D. Zhu, J. Liu, Y. Zhao, Y. Zheng, S.-Z. Qiao, *Small* **2019**, *15*, 1805511; n) G. Zhan, H. C. Zeng, *Adv. Funct. Mater.* **2016**, *26*, 3268; o) Q. Zuo, T. Liu, C. Chen, Y. Ji, X. Gong, Y. Mai, Y. Zhou, *Angew. Chem., Int. Ed.* **2019**, *58*, 10198; p) M. Liu, K. Xie, M. D. Nothling, P. A. Gurr, S. S. L. Tan, Q. Fu, P. A. Webley, G. G. Qiao, *ACS Nano* **2018**, *12*, 11591; q) R. Yan, Y. Zhao, H. Yang, X.-J. Kang, C. Wang, L.-L. Wen, Z.-D. Lu, *Adv. Funct. Mater.* **2018**, *28*, 1802021; r) X. Zhang, P. Zhang, C. Chen, J. Zhang, G. Yang, L. Zheng, J. Zhang, B. Han, *Green Chem.* **2019**, *21*, 54; s) A. Pustovarenko, M. G. Goesten, S. Sachdeva, M. Shan, Z. Amghouz, Y. Belmabkhout, A. Dikhtiarenko, T. Rodenas, D. Keskin, I. K. Voets, B. M. Weckhuysen, M. Eddaoudi, L. C. P. M. de Smet, E. J. R. Sudhölter, F. Kapteijn, B. Seoane, J. Gascon, *Adv. Mater.* **2018**, *30*, 1707234; t) H. Fan, H. Yu, X. Wu, Y. Zhang, Z. Luo, H. Wang, Y. Guo, S. Madhavi, Q. Yan, *ACS Appl. Mater. Interfaces* **2016**, *8*, 25261; u) Y. Lin, H. Wan, D. Wu, G. Chen, N. Zhang, X. Liu, J. Li, Y. Cao, G. Qiu, R. Ma, *J. Am. Chem. Soc.* **2020**, *142*, 7317; v) G. Chen, S. Huang, X. Kou, F. Zhu, G. Ouyang, *Angew. Chem., Int. Ed.* **2020**, *59*, 13947.
[45] a) S. Motoyama, R. Makiura, O. Sakata, H. Kitagawa, *J. Am. Chem. Soc.* **2011**, *133*, 5640; b) R. Makiura, R. Usui, Y. Sakai, A. Nomoto, A. Ogawa, O. Sakata, A. Fujiwara, *ChemPlusChem* **2014**, *79*, 1352; c) G. Xu, T. Yamada, K. Otsubo, S. Sakaida, H. Kitagawa, *J. Am. Chem. Soc.* **2012**, *134*, 16524.
[46] A. Dmitriev, H. Spillmann, N. Lin, J. V. Barth, K. Kern, *Angew. Chem., Int. Ed.* **2003**, *42*, 2670.
[47] T. Tsuruoka, S. Furukawa, Y. Takashima, K. Yoshida, S. Isoda, S. Kitagawa, *Angew. Chem., Int. Ed.* **2009**, *48*, 4739.
[48] a) M.-H. Pham, G.-T. Vuong, F.-G. Fontaine, T.-O. Do, *Cryst. Growth Des.* **2012**, *12*, 3091; b) P. Nian, H. Liu, X. Zhang, *CrystEngComm* **2019**, *21*, 3199.
[49] a) S. Wang, T. Wang, H. Zheng, F. Fan, Z. Gu, W. He, B. Zhang, L. Shao, H. Chen, Y. Li, X. Zhang, L. Zhang, Y. Fu, W. Qi, *Microporous Mesoporous Mater.* **2020**, *303*, 110254; b) Z. Wang, G. Wang, H. Qi, M. Wang, M. Wang, S. Park, H. Wang, M. Yu, U. Kaiser, A. Fery, S. Zhou, R. Dong, X. Feng, *Chem. Sci.* **2020**, *11*, 7665.
[50] R. Xu, M. Jian, Q. Ji, C. Hu, C. Tang, R. Liu, X. Zhang, J. Qu, *Chem. Eng. J.* **2020**, *382*, 122658.
[51] H. Sun, K.-Z. Wang, M.-R. Yao, C.-X. Yu, Y.-H. Song, J. Ding, Y.-L. Zhou, D. Liu, L.-L. Liu, *Inorg. Chem. Front.* **2023**, *10*, 6566.
[52] J. Huang, S. Zhou, S. Zhang, L. Wang, X.-T. Wu, Q.-L. Zhu, Y. Wen, *Sep. Purif. Technol.* **2024**, *336*, 126294.
[53] J. Li, Q. Duan, Z. Wu, X. Li, K. Chen, G. Song, A. Alsaedi, T. Hayat, C. Chen, *Chem. Eng. J.* **2020**, *383*, 123189.
[54] S. Gai, R. Fan, J. Zhang, X. Zhou, K. Xing, K. Zhu, W. Jia, W. Sui, P. Wang, Y. Yang, *J. Mater. Chem. A* **2021**, *9*, 3369.
[55] C. Duan, L. Dong, F. Li, Y. Xie, B. Huang, K. Wang, Y. Yu, H. Xi, *Ind. Eng. Chem. Res.* **2020**, *59*, 18857.
[56] C. Li, X. Zhang, S. Wen, R. Xiang, Y. Han, W. Tang, T. Yue, Z. Li, *J. Hazard. Mater.* **2020**, *395*, 122615.
[57] H. Li, K. Gao, B. Mo, Q. Meng, K. Li, J. Wu, H. Hou, *Dalton Trans.* **2021**, *50*, 3348.
[58] N. Ahmad, H. A. Younus, A. H. Chughtai, K. Van Hecke, Z. A. K. Khattak, Z. Gaoke, M. Danish, F. Verpoort, *Catal. Sci. Technol.* **2018**, *8*, 4010.
[59] M. Zhang, Z. Qi, Y. Feng, B. Guo, Y. Hao, Z. Xu, L. Zhang, D. Sun, *Inorg. Chem. Front.* **2018**, *5*, 1314.
[60] T.-G. Qu, X.-M. Hao, H. Wang, X.-G. Cui, F. Chen, Y.-B. Wu, D. Yang, M. Zhang, W.-L. Guo, *Polyhedron* **2018**, *156*, 208.
[61] Y. Li, H.-H. Yuan, C.-P. Li, J. Li, *Inorg. Chem. Commun.* **2017**, *80*, 36.
[62] S. Zhao, S. Li, Z. Zhao, Y. Su, Y. Long, Z. Zheng, D. Cui, Y. Liu, C. Wang, X. Zhang, Z. Zhang, *Environ. Sci. Pollut. Res.* **2020**, *27*, 39186.
[63] J. Yan, Y. Li, Y. Li, S. Ouyang, T. Zhang, *PhotoMat* **2023**, 1.
[64] Y. Pan, R. Abazari, J. Yao, J. Gao, *J. Phys.: Energy* **2021**, *3*, 032010.
[65] J.-P. Dong, Z.-Z. Shi, B. Li, L.-Y. Wang, *Dalton Trans.* **2019**, *48*, 17626.
[66] X. Ding, H. Liu, J. Chen, M. Wen, G. Li, T. An, H. Zhao, *Nanoscale* **2020**, *12*, 9462.
[67] J. Li, X. Li, G. Wu, J. Guo, X. Yin, M. Mu, *J. Environ. Chem. Eng.* **2021**, *9*, 106723.
[68] K. Bhuvaneswari, G. Palanisamy, T. Pazhanivel, T. Maiyalagan, P. Shanmugam, A. N. Grace, *Chemosphere* **2021**, *270*, 128616.
[69] J. Zhou, H. Tang, C. Yao, W. Song, C. Liu, W. Song, Z. Zhang, *Sustain. Mater. Technol.* **2024**, *39*, e00825.
[70] J.-Y. Tian, W.-C. Lv, A.-S. Shen, Y. Ma, M. Wang, S. Zhang, X.-L. Liu, Z. Zhang, M. Du, *Sep. Purif. Technol.* **2023**, *327*, 124903.
[71] S. Kim, H. Wang, Y. M. Lee, *Angew. Chem., Int. Ed.* **2019**, *58*, 17512.
[72] W. Fan, Y. Ying, S. B. Peh, H. Yuan, Z. Yang, Y. D. Yuan, D. Shi, X. Yu, C. Kang, D. Zhao, *J. Am. Chem. Soc.* **2021**, *143*, 17716.
[73] Y. Liu, H. Chen, T. Li, Y. Ren, H. Wang, Z. Song, J. Li, Q. Zhao, J. Li, L. Li, *Angew. Chem., Int. Ed.* **2023**, *62*, 202309095.
[74] M. Kalaj, K. C. Bentz, S. Ayala Jr., J. M. Palomba, K. S. Barcus, Y. Katayama, S. M. Cohen, *Chem. Rev.* **2020**, *120*, 8267.
[75] X. Ma, Y. Chai, P. Li, B. Wang, *Acc. Chem. Res.* **2019**, *52*, 1461.
[76] S. Datta, A. Mayoral, S. Bettahalli, P. Bhatt, M. Karunakaran, I. Carja, D. Fan, P. G. M Mileo, R. Semino, G. Maurin, O. Terasaki, M. Eddaoudi, *Science* **2022**, *376*, 1080.
[77] M. Jian, R. Qiu, Y. Xia, J. Lu, Y. Chen, Q. Gu, R. Liu, C. Hu, J. Qu, H. Wang, X. Zhang, *Sci. Adv.* **2020**, *6*, eaay3998.
[78] P. Cheng, Y. Huang, C. Wu, X. Wang, X. Fu, P. Li, Y. Liu, S. Xia, *J. Membr. Sci.* **2021**, *640*, 119812.
[79] H. Yuan, K. Li, D. Shi, H. Yang, X. Yu, W. Fan, P. J. S. Buenconsejo, D. Zhao, *Adv. Mater.* **2023**, *35*, 2211859.
[80] Y. Zhang, L. Yang, X. Tian, J. Qiu, L. Jiang, J. Qiu, *Chem. Eng. J.* **2024**, *484*, 149504.

[81] Y. Liu, X.-p. Wang, Z.-a. Zong, R. Lin, X.-y. Zhang, F.-s. Chen, W.-d. Ding, L.-l. Zhang, X.-m. Meng, J. Hou, *J. Membr. Sci.* **2022**, *653*, 120520.
[82] a) P. Zhao, J. Wang, X. Han, J. Liu, Y. Zhang, B. Van der Bruggen, *Ind. Eng. Chem. Res.* **2021**, *60*, 1850; b) Z. Wang, R. Su, Z. Liu, Y. Chen, B. Gao, Z. Wang, Q. Li, *Desalin. Water Treatm.* **2021**, *228*, 121.
[83] J. Dong, D. Zhao, Y. Lu, W.-Y. Sun, *J. Mater. Chem. A* **2019**, *7*, 22744.
[84] M. Zhang, G. Feng, Z. Song, Y.-P. Zhou, H.-Y. Chao, D. Yuan, T. T. Y. Tan, Z. Guo, Z. Hu, B. Z. Tang, B. Liu, D. Zhao, *J. Am. Chem. Soc.* **2014**, *136*, 7241.
[85] P. Chen, X. Su, C. Wang, G. Zhang, T. Zhang, G. Xu, L. Chen, *Angew. Chem., Int. Ed.* **2023**, *62*, 202306224.
[86] H. Xu, J. Gao, X. Qian, J. Wang, H. He, Y. Cui, Y. Yang, Z. Wang, G. Qian, *J. Mater. Chem. A* **2016**, *4*, 10900.
[87] V. K. Maka, A. Mukhopadhyay, G. Savitha, J. N. Moorthy, *Nanoscale* **2018**, *10*, 22389.
[88] C. Park, J. W. Baek, E. Shin, I.-D. Kim, *ACS Nanosci. Au* **2023**, *3*, 353.
[89] M. K. Smith, K. A. Mirica, *J. Am. Chem. Soc.* **2017**, *139*, 16759.
[90] Z. Meng, A. Aykanat, K. A. Mirica, *J. Am. Chem. Soc.* **2019**, *141*, 2046.
[91] V. Rubio-Giménez, N. Almora-Barrios, G. Escorcia-Ariza, M. Galbiati, M. Sessolo, S. Tatay, C. Martí-Gastaldo, *Angew. Chem., Int. Ed.* **2018**, *57*, 15086.
[92] M. S. Yao, X. J. Lv, Z. H. Fu, W. H. Li, W. H. Deng, G. D. Wu, G. Xu, *Angew. Chem., Int. Ed.* **2017**, *56*, 16510.
[93] D. Han, X. Liu, S. Wu, *Chem. Soc. Rev.* **2022**, *51*, 7138.
[94] I. Abánades Lázaro, X. Chen, M. Ding, A. Eskandari, D. Fairen-Jimenez, M. Giménez-Marqués, R. Gref, W. Lin, T. Luo, R. S. Forgan, *Nat. Rev. Methods Primers* **2024**, *4*, 42.
[95] J. Li, Z. Cui, Y. Zheng, X. Liu, Z. Li, H. Jiang, S. Zhu, Y. Zhang, P. K. Chu, S. Wu, *Appl. Catal., B* **2022**, *317*, 121701.
[96] S. Marqus, H. Ahmed, A. R. Rezk, T. Huynh, A. Lawrie, D. Nguyen, Y. Ehrnst, C. Dekiwadia, L. Y. Yeo, *ACS Appl. Mater. Interfaces* **2021**, *13*, 58309.
[97] Z. Wang, J. Zhu, S. Xu, Y. Zhang, B. Van der Bruggen, *J. Membr. Sci.* **2021**, *633*, 119397.
[98] J. Li, S. Song, J. Meng, L. Tan, X. Liu, Y. Zheng, Z. Li, K. W. K. Yeung, Z. Cui, Y. Liang, S. Zhu, X. Zhang, S. Wu, *J. Am. Chem. Soc.* **2021**, *143*, 15427.
[99] J.-H. Qin, H. Zhang, P. Sun, Y.-D. Huang, Q. Shen, X.-G. Yang, L.-F. Ma, *Dalton Trans.* **2020**, *49*, 17772.

Lun Lu completed his Ph.D. and continued 2-year postdoctoral research at Zhejiang University from 2015–2021. He then joined the South China Institute of Environmental Science (SCIES), Ministry of Ecology and Environment, and was appointed as Associate Professor in 2022. His research interests are related to the design and synthesis of materials and devices for environmental protection, and has published more than 30 SCI papers in referenced journals.

Liangzhong Li is currently a professor at the Guangzhou Institute of Energy Conversion (GIEC), Chinese Academy of Sciences. He received his Ph.D. degree from the East China University of Science and Technology in 2021 and served as a faculty member in SCIES during 2016–2018 and 2021–2023. His research has focused on the synthesis of advanced adsorbents, catalysts, and membranes for various purposes. To date, he has published 50 publications in international journals and 4 book chapters.

Cheng Chen obtained his Ph.D. degree from the College of Environmental and Resource Sciences of Zhejiang University in 2021. He is now a researcher at Zhejiang Normal University. His main research interests are the development and environmental application of functional membrane materials. He has published over 40 articles in famous journals such as EST, WR, and so on.

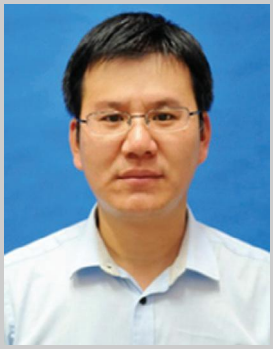

Hongjun Lin is the dean of the College of Geography and Environmental Sciences at Zhejiang Normal University. He obtained his Ph.D. degree from the Shanghai Institute of Applied Physics from the Chinese Academy of Sciences in 2006. As the group leader, his research interests are membrane separation technology, catalysis, and mechanism research. He has published more than 300 SCI papers with more than 20 000 citations, and the h-index is 79.